NATIONAL ADVISORY COMMITTEE FOR AERONAUTICS

TECHNICAL NOTE 3436

AN INVESTIGATION OF SEVERAL NACA 1-SERIES NOSE INLETS WITH AND WITHOUT PROTRUDING CENTRAL BODIES AT HIGH-SUBSONIC MACH NUMBERS AND AT A MACH NUMBER OF 1.2

By Robert E. Pendley and Harold L. Robinson

Langley Aeronautical Laboratory
Langley Field, Va.

Washington
May 1955

NATIONAL ADVISORY COMMITTEE FOR AERONAUTICS

TECHNICAL NOTE 3436

AN INVESTIGATION OF SEVERAL NACA 1-SERIES NOSE INLETS WITH AND WITHOUT PROTRUDING CENTRAL BODIES AT HIGH-SUBSONIC MACH NUMBERS AND AT A MACH NUMBER OF 1.2[1]

By Robert E. Pendley and Harold L. Robinson

SUMMARY

An investigation of three NACA 1-series nose inlets, two of which were fitted with protruded central bodies, was conducted in the Langley 8-foot high-speed tunnel. An elliptical-nose body, which had a critical Mach number approximately equal to that of one of the nose inlets, was also tested. Tests were made near zero angle of attack for a Mach number range from 0.4 to 0.925 and for the supersonic Mach number of 1.2. The inlet-velocity-ratio range extended from zero to a maximum value of 1.34. Measurements included pressure distribution, external drag, and total-pressure loss of the internal flow near the inlet. Drag was not measured for the tests at the supersonic Mach number.

Over the range of inlet-velocity ratio investigated, the calculated external pressure-drag coefficient at a Mach number of 1.2 was consecutively lower for the nose inlets of higher critical Mach number, and the pressure-drag coefficient of the longest nose inlet was in the range of pressure-drag coefficient for two solid noses of fineness ratio 2.4 and 6.0. For Mach numbers below the Mach number of the supercritical drag rise, extrapolation of the test data indicated that the external drag of the nose inlets was little affected by the addition of central bodies at or slightly below the minimum inlet-velocity ratio for unseparated central-body flow. The addition of central bodies to the nose inlets also led to no appreciable effects on either the Mach number of the supercritical drag rise, or, for inlet-velocity ratios high enough to avoid a pressure peak at the inlet lip, on the critical Mach number. The total-pressure recovery of the inlets tested, which were of a subsonic type, was sensibly unimpaired at the supersonic Mach number of 1.2. Low-speed measurements of the minimum inlet-velocity ratio for unseparated central-body flow appear to be applicable for Mach numbers extending to 1.2.

---

[1]Supersedes recently declassified NACA RM L9L23a, 1950.

INTRODUCTION

The development of a series of nose inlets for application to high-speed aircraft is reported in reference 1. This series of nose inlets, designated as the NACA 1-series, was investigated later (reference 2) with protruded central bodies suitable for propeller spinners or accessory housings. Since the tests of references 1 and 2 were conducted principally at low speeds, high-speed characteristics were predicted from low Mach number data.

A subsequent investigation has therefore been undertaken for the purpose of studying the aerodynamic characteristics of NACA 1-series nose inlets at supercritical speeds. The surface pressure-distribution and external-drag characteristics of three representative nose inlets of the series are reported in reference 3 for Mach numbers extending up to 0.925. The present paper reports for these nose inlets a study of additional pressure distributions and a study of the effects of several protruded central bodies on the external pressure distribution, the external drag, and the total-pressure losses of the internal flow. The nose-inlet pressure distributions were measured for Mach numbers of approximately 0.4, 0.8, and 1.2, and central-body effects were investigated for a range of Mach number from 0.4 to 0.925 and at a Mach number of 1.2. An elliptical-nose body was also tested for the purpose of comparing the pressure distribution of an NACA 1-series nose inlet with that of a solid streamline nose at transonic speeds.

SYMBOLS

A	duct area
C_{D_e}	external drag coefficient, based on maximum nose-inlet frontal area
C_{D_p}	external pressure-drag coefficient, based on maximum nose-inlet frontal area
D	nose-inlet maximum diameter
F_e	resultant of pressure forces acting on external surface, positive in drag direction
F_i	resultant of pressure forces acting on internal surface, positive in drag direction
H	total pressure

ΔH	total-pressure decrement from free stream to inlet rake station
m	internal mass-flow rate
M	Mach number
M_{cr}	critical Mach number, free-stream Mach number at which local sonic velocity is first attained
p	static pressure
P	pressure coefficient, $\frac{p - p_o}{q_o}$
P_{cr}	critical pressure coefficient, corresponding to local Mach number of 1.0
q	dynamic pressure, $\frac{1}{2}\rho V^2$
r	radius, measured from nose-inlet center line
r_L	nose-inlet lip radius, in.
r_m	radius of nose-inlet diffuser wall at entrance rake station, measured from nose-inlet center line
r_s	radius of central body, measured from nose-inlet center line
V	velocity
x	axial distance from inlet station, positive rearward, in.
x_e	axial distance from nose of ellipsoid, in.
y	ordinate measured perpendicular to reference line, in.
$\left(\frac{\Delta H}{H_o - p_o}\right)_{av}$	average total-pressure-loss coefficient, $\frac{1}{A_d}\int_{A_d}\left(\frac{\Delta H}{H_o - p_o}\right)dA_d$
α	angle of attack of nose-inlet center line, deg
θ	angle of nose-inlet diffuser wall measured from reference line (fig. 3)
ρ	air mass density

Subscripts:

o	free stream
1	nose-inlet entrance
d	inlet rake station
j	jet

APPARATUS AND TESTS

The investigation was made in the Langley 8-foot high-speed tunnel and involved the use of two different test sections and model support systems. One arrangement (described in reference 3) consisted of a sting-strut support system mounted in the conventional subsonic test section. A photograph of this installation is given as figure 1(a). The other arrangement consisted of the model support system, shown schematically in figure 1(b) with the models mounted in the 1.20 (nominal) Mach number supersonic test section. The supersonic test section had a circular cross section with a diameter of approximately 94 inches. Mach number distributions along the center line with the tunnel empty are given in figure 2.

Models.- The three NACA 1-series nose inlets tested are designated, after the method of reference 1, as the NACA 1-65-050, NACA 1-50-100, and NACA 1-40-200 nose inlets. These inlets represent a critical-speed cross section of the NACA 1-series nose inlets. Design critical Mach number and design (minimum) inlet-velocity ratio measured for these nose inlets in the low-speed tests of reference 1 are given in the following table:

NACA nose inlet	M_{cr}	$(V_1/V_o)_{min}$
1-65-050	0.700	0.18
1-50-100	.795	.20
1-40-200	.875	.40

The nose-inlet models used in the present investigation were previously used in the tests of reference 3. Two of these inlets, the NACA 1-65-050 and NACA 1-50-100 nose inlets, were tested with central bodies representative of propeller spinners or accessory housings.

The tests also included an elliptical nose which consisted of half an ellipsoid of fineness ratio (major-to-minor-axis ratio) 2.4. The critical Mach number of this nose was approximately equal to the design critical Mach number of the NACA 1-50-100 nose inlet. A drawing of the model combinations tested is shown in figure 3, and the central-body ordinates are given in figure 4.

The central-body diameters at the inlet were such as to raise the inlet-velocity ratio from the design minimum value for the open nose inlet to approximately 0.35 at the nose-inlet design mass-flow rate. Central bodies A and D, which were tested with the NACA 1-65-050 and NACA 1-50-100 nose inlets, respectively, were ellipsoids with a major-to-minor-axis ratio of 3. In addition to the elliptical central body, two conical-type central bodies, designated as central bodies B and C, were also tested with the NACA 1-65-050 nose inlet. These central bodies had 60° conical noses and were of equal diameter at the inlet, but differed in the amount of protrusion and in the manner in which the conical surface was faired into the surface of zero slope at the inlet. The transition surfaces were of a parabolic profile for each central body, but the distance from the inlet to the point of tangency of the conical surface and the parabolic surface was set equal to the inlet-annulus width for central body B and to twice the inlet-annulus width for central body C. For both conical central bodies, the axis of the parabolic portion of the profile was contained in the inlet plane.

Tests in subsonic test section.- For the tests in the subsonic test section, the nose inlets were mounted on the NACA 111 afterbody shown in figure 5(a), which was previously used in the tests of reference 3. Data were recorded for a range of Mach number from approximately 0.4 to 0.925. The corresponding Reynolds number range, based on nose-inlet maximum diameter, extended from approximately 610,000 to 940,000 (reference 3). The angle of attack was near zero, but varied among the models from -0.3° to 0.1°.

The same measurements reported in reference 3 were made during the tests in the subsonic test section. Nose-inlet pressure distribution was measured by a row of pressure orifices on the upper surface lying in a vertical plane through the axis, and the external drag was measured by a wake-survey rake (fig. 1(a)). Inlet-velocity ratio was calculated from measurements made with a rake of total-pressure and static-pressure tubes which spanned a venturi throat in the internal-flow ducting as described in reference 3. The minimum value of the inlet-velocity ratio for the tests in the subsonic test section was zero and the maximum value, which depended on the Mach number and model configuration, was approximately 0.6.

Tests in supersonic test section.- For the tests in the supersonic test section, the models were mounted on a 3.5-inch-diameter tube

suspended along the axis of the tunnel, as shown in figure 1(b). The connecting members between this tube and the inlet models are shown in figure 5(b). In addition to tests at a Mach number of 1.2, (Reynolds number, approximately 980,000) tests were also made in the supersonic test section at Mach numbers of approximately 0.4 and 0.8, for which Mach number gradients at the model were small (fig. 2). All tests in the supersonic test section were made at zero angle of attack.

Measurements of nose-inlet pressure distribution, internal mass-flow rate, and total-pressure loss near the inlet were made during the tests in the supersonic test section. As shown in figure 1(b), the internal flow was ducted through the 3.5-inch-diameter tube located along the tunnel axis, and exhausted through a throttle into the tunnel diffuser. Inlet-velocity ratio was calculated from measurements made with a rake of total-pressure and static-pressure tubes in the venturi throat shown in figure 5(b). The inlet-velocity-ratio range of these tests extended from zero to a maximum value of 1.34. Total pressure near the inlet was measured for the NACA 1-65-050 and NACA 1-50-100 nose-inlet - central-body combinations by total-pressure rakes mounted at the stations indicated in figure 3.

METHODS AND PRECISION

The values of inlet-velocity ratio given in this paper are nominal values calculated from the mass flow and inlet area. Isentropic flow was assumed from the free stream to the inlet for subsonic Mach numbers, and a normal shock was assumed ahead of the inlet for the supersonic Mach number, with isentropic flow from the shock to the inlet. These assumptions are valid for nose inlets under the conditions of the tests reported herein, but the flow entering the inlet of nose-inlet - central-body combinations without boundary-layer control departs appreciably from isentropic conditions. However, for the combinations of inlet-velocity ratio and inlet total-pressure loss of these tests, an analysis showed that the largest error in the calculated value of the inlet-velocity ratio caused by neglecting the inlet total-pressure loss was approximately 0.02.

Condensation of water vapor in the test section was present during some of the tests at the supersonic Mach number. This condensation reduced the test Mach number by approximately 0.02. The maximum effect of tunnel-wall constriction on the test Mach number at subsonic Mach numbers was less than 1 percent. Because of the small magnitude of condensation and wind-tunnel-wall corrections to the data of these tests, no corrections have been applied.

All data were obtained in the tests from pressure measurements and the most likely source of error in the measurements resulted from the practice of reading the manometer-liquid height to the nearest manometer scale graduation. The maximum error in pressure coefficient caused by this practice was at the lowest test Mach number and was approximately ±0.005. The error in drag coefficient, which was a function of Mach number and wake width, was less than approximately ±6 percent at the lowest Mach number, ±2 percent at the critical Mach number, and ±4 percent at the highest subsonic Mach number and wake-width condition of the tests.

The computation of inlet-velocity ratio was least accurate at the lowest inlet-velocity ratios, lowest Mach number, and for the inlet of the least area. Accordingly, at inlet-velocity ratios of 0.1 and lower, the calculated values of inlet-velocity ratio could have ranged from 0 to 0.2; whereas at inlet-velocity ratios of 0.3 and higher, the error in inlet-velocity ratio was less than approximately ±0.04. These errors in inlet-velocity ratio are believed to have no significant effect on the conclusions of this paper.

RESULTS AND DISCUSSION

Nose Inlets

Surface pressure distributions.- The surface pressure distributions presented in figure 6 were measured during the tests in the supersonic test section. Negligible differences were found between the pressure distributions measured at subsonic Mach numbers during these tests and those measured at comparable Mach numbers and inlet-velocity ratios for the model support system which was used for the tests in the subsonic test section. The pressure distributions of figure 6 for subsonic Mach numbers are therefore valid for nose inlets mounted on afterbodies similar to the afterbody used for the tests in the subsonic test section.

The subsonic nose-inlet pressure distributions of figure 6 are in essential agreement with the pressure distributions discussed in reference 3. Some modifications to the discussion of the characteristics of the NACA 1-65-050 nose inlet in reference 3 are necessary, however, as a result of data obtained with an additional pressure orifice used in the present tests. It was stated in reference 3 that the pressure peak induced at the lip of the NACA 1-65-050 nose inlet by low inlet-velocity ratios at low Mach numbers was absent at and above the critical Mach number. As shown in figure 6(a), however, a pressure peak near the inlet lip is indicated by the additional pressure orifice $\left(\frac{x}{D} = 0.06\right)$ at

zero inlet-velocity ratio for the supercritical Mach number of 0.81. The reduction of inlet-velocity ratio to zero has therefore more effect on the critical Mach number of the NACA 1-65-050 nose inlet than was indicated in reference 3. Because of the limited number of pressure orifices available on the small-scale models of the tests, critical Mach number cannot be accurately measured for conditions for which the lowest surface pressure exists as a sharp peak. Fortunately, however, knowledge of the critical Mach number at low inlet-velocity ratios for the NACA 1-65-050 nose inlet is relatively unimportant inasmuch as the drag measurements of reference 3 showed for this nose inlet no effect of inlet-velocity ratio on the Mach number of the supercritical drag rise, and, furthermore, only a small effect of inlet-velocity ratio on drag coefficient was shown throughout the Mach number range of the tests.

At inlet-velocity ratios for which the pressure gradient is favorable from the nose-inlet lip to the maximum diameter, the pressure distributions of all three nose inlets at the supersonic Mach number (figs. 6(a), 6(e), and 6(g)) are somewhat similar to the pressure distributions for subcritical Mach numbers. However, the pressures for the supersonic Mach number are more positive over the forward part of the inlet, and the position of the negative peak-pressure coefficient and the point at which the pressure coefficient has returned to zero have moved farther rearward. From the point of minimum pressure near the nose-inlet maximum diameter, the flow is gradually recompressed to free-stream pressure.

The maximum induced velocities at the supersonic Mach number vary with nose-inlet proportions in the same manner as for subsonic Mach numbers: the maximum induced velocity is lower for the nose inlets of higher critical Mach number. The reduction of the inlet-velocity ratio to zero led to a pressure peak at the inlet lip only for the NACA 1-40-200 nose inlet.

A comparison of the pressure coefficients on the elliptical nose and the NACA 1-50-100 nose inlet at selected inlet-velocity ratios is shown in figure 7 with the pressures plotted at equal distances from the maximum-diameter station. Although the shapes of the pressure distributions forward of the point of maximum induced velocity are similar, the pressures over the nose inlet are more positive than those for the elliptical nose in this region. The compression of the flow rearward from the point of maximum induced velocity appears to be somewhat more rapid for the elliptical nose at the two subsonic Mach numbers and distinctly more rapid at the supersonic Mach number.

Supersonic pressure drag.- External nose-inlet pressure drag has been evaluated from the supersonic pressure distributions of the nose inlets. The external pressure drag of a nose inlet is obtained by consideration of a hypothetical body consisting of the nose inlet with

a long, tapering afterbody, the taper being so gradual that the pressure on the afterbody is stream pressure (fig. 8). The external pressure drag is then defined as the sum of the dragwise components of the pressure forces acting externally and internally on the body minus the internal drag resulting from the total-pressure loss of a normal shock assumed ahead of the inlet. This relationship is given by the following expression:

$$D_p = F_e + F_i - m(V_o - V_j)$$

The force F_e was obtained by integration of the measured pressures acting on the nose inlet and the free-stream pressure assumed to be acting on the afterbody. In calculating the force F_i, the internal flow was assumed isentropic downstream from the normal shock. The exit area of the internal-flow duct could then be calculated as a function of inlet-velocity ratio from the internal mass-flow rate and the assumption of free-stream pressure acting at the exit. Given the internal mass-flow rate and inlet-velocity ratio, the resultant force F_i acting on the internal surface of the body was then calculated from the momentum and pressure of the flow at the inlet and exit:

$$F_i = p_1 A_1 - p_o A_j - m(V_j - V_1)$$

The external pressure-drag coefficients of the three nose inlets obtained in this manner are plotted in figure 8 as a function of inlet-velocity ratio. The external pressure drag calculated by the preceding method is exactly equal to the value given by the sum of the external and additive drags of reference 4.

The pressure-drag coefficients of two solid bodies with elliptical noses are also given in figure 8 for the sake of comparison. These drag coefficients were calculated with the assumption of the same type of hypothetical afterbody assumed for the nose-inlet calculations. Obviously, for the elliptical noses, the afterbody was closed so that the pressure-drag calculation became simply an integration of the measured pressures over the noses and the free-stream pressure assumed acting over the afterbody. The drag coefficient given in figure 8 for the ellipsoid fineness ratio of 2.4 was obtained from integration of the supersonic pressure distribution of the elliptical nose of figure 7. The drag coefficient indicated for the ellipsoid fineness ratio of 6.0 was obtained from integration of the pressure distribution for a Mach number of 1.2 over the forebody of the ellipsoid used in the tests of reference 5.

Inspection of figure 8 shows that, over the range of test inlet-velocity ratio, the external pressure-drag coefficient was consecutively lower for the nose inlets of greater length ratio. The nose-inlet

length ratio cannot by itself serve as an index of the pressure drag, but for the range of inlet diameters involved in the three nose inlets tested, the length ratio is the more definitive parameter. For each nose inlet, the drag coefficient diminished with increasing inlet-velocity ratio, but tended to diminish more gradually at the higher inlet-velocity ratios. The pressure-drag coefficient of the longest nose inlet at useful inlet-velocity ratios is shown to be within the range of pressure-drag coefficient for the two solid noses.

Nose-Inlet - Central-Body Combinations

Surface pressure distributions.- Nose-inlet pressure distributions are given in figures 6(b), 6(c), and 6(d) for the NACA 1-65-050 nose inlet with an elliptical and two conical central bodies. Pressure distributions for the NACA 1-50-100 nose inlet with an elliptical central body are given in figure 6(f). Comparisons of the nose-inlet pressure distributions of the NACA 1-65-050 nose inlet with those for the inlet fitted with each of the three central bodies are shown in figures 9 and 10, as measured in the supersonic and subsonic test sections, respectively. A similar comparison is given for the NACA 1-50-100 nose inlet in figure 11. The inlet-velocity ratios given for the comparison of figures 9 and 11 are the lowest and highest values available for comparison, whereas the inlet-velocity ratio of figure 10 was selected to obtain a pressure distribution without a peak at the inlet lip. The addition of any of the central bodies at a given inlet-velocity ratio led to only a small effect on the nose-inlet pressure distribution for all Mach numbers. The apparent effect of central body A on the pressure distribution of the NACA 1-65-050 nose inlet (fig. 10) is believed to have been caused by a discrepancy in the angle of attack for the test of this central body. Thus the critical Mach number of the nose inlets may be assumed to be the critical Mach number of the nose-inlet - central-body combinations. Furthermore, the small effect of central bodies on the pressure near maximum diameter indicates little effect of spinners on the characteristics of the supercritical drag rise.

External drag.- The external drag coefficient is presented for selected Mach numbers as a function of inlet-velocity ratio in figures 12 and 13 for the NACA 1-65-050 and NACA 1-50-100 nose inlets with and without central bodies. At Mach numbers below the Mach number of the supercritical drag rise, the effect of inlet-velocity ratio on the drag coefficient was small for all configurations except the NACA 1-65-050 nose inlet with central body C (fig. 12(d)) and the NACA 1-50-100 nose inlet with central body D (fig. 13(b)), for which cases an appreciable increase in drag resulted when the inlet-velocity ratio was reduced from approximately 0.35 to the lowest test values.

Comparisons of the external drag of the NACA 1-65-050 and NACA 1-50-100 nose inlets with the external drag of these inlets fitted with central bodies are presented in figures 14 and 15. These curves were obtained from faired plots illustrated in figures 12 and 13, and the inlet-velocity ratios chosen for the comparisons are the lowest and highest values for which the data permit a satisfactory comparison. The measured critical Mach numbers are indicated for each configuration. As previously mentioned, the critical Mach numbers indicated for the lower inlet-velocity ratios were not accurately measurable. The critical Mach number indicated for central body A at 0.2 inlet-velocity ratio (fig. 14) is believed to be higher than those indicated for the conical central bodies and the nose inlet alone as a result of the small negative angle of attack (-0.3°) for the test of this central body. As previously inferred from the pressure-distribution measurements and as verified by the drag curves for the NACA 1-65-050 nose inlet with central bodies B and C (fig. 14), the central bodies had little effect on the supercritical drag characteristics. Drag data for the tests with elliptical central bodies are presented only up to Mach numbers slightly greater than the critical Mach number because a wake-survey rake of length adequate to measure the shock losses was not available at the time of those tests.

For both inlet-velocity ratios and for Mach numbers below the Mach number of the supercritical drag rise, the drag comparisons of figure 14 indicate that the external drag of the NACA 1-65-050 nose inlet was little affected by the presence of the elliptical central body A, whereas the drag was increased somewhat by the presence of both the conical central bodies B and C. The external drag of the NACA 1-50-100 nose inlet (fig. 15) was increased by the presence of the elliptical central body D for both inlet-velocity ratios.

As will be shown later, the higher inlet-velocity ratios given for the drag comparisons of figures 14 and 15 are lower than the minimum values desirable from the standpoint of internal-flow pressure recovery. For the Mach number range extending to slightly beyond the critical Mach number, some indication of the effect of central bodies on the external drag coefficient at higher inlet-velocity ratios may be obtained from reference to figures 12 and 13. The higher inlet-velocity ratios given for the drag comparisons of figures 14 and 15 were limited by the inlet-velocity-ratio range for the nose-inlet-alone tests. However, a consideration of the effects on the external pressure distribution resulting from increasing the inlet-velocity ratio beyond the design minimum value leads to the belief that, for the NACA 1-65-050 and NACA 1-50-100 nose inlets, little change would occur in the drag coefficients if the inlet-velocity ratio were increased to the maximum values obtained for the tests with the central bodies. If then the values of the drag coefficients shown in figures 12(a) and 13(a) for the highest test inlet-velocity ratios and for Mach numbers below the Mach number of the

supercritical drag rise are extended to higher inlet-velocity ratios, it can be seen that these values are little different from the values of the drag coefficients measured for the nose-inlet - central-body combinations at inlet-velocity ratios of approximately 0.4. This value of inlet-velocity ratio is slightly lower than the minimum inlet-velocity ratio for unseparated central-body flow, which will be discussed subsequently.

Internal flow.- For nose-inlet - central-body combinations, a minimum inlet-velocity ratio exists below which the central-body boundary layer separates under the influence of the pressure rise ahead of the inlet. Minimum inlet-velocity ratios for the NACA 1-series spinners, which are similar to ellipsoidal central bodies, are given in reference 2. It was found in reference 2 that the adverse pressure rise acting on the central-body boundary layer ahead of the inlet could be reduced by the use of a central body which, ahead of the inlet, had the shape of a right circular cone. For a given inlet diameter, however, the volume of a conical central body available for housing propeller hubs or engine accessories will be less than that of a conventional central body with a profile similar to an ellipse. The two central bodies B and C were therefore designed for tests with the NACA 1-65-050 nose inlet to determine if a modification could be made to a conical central body to increase its volume without seriously affecting the minimum inlet-velocity ratio for unseparated central-body flow.

The results of the internal-flow total-pressure measurements at the stations indicated in figure 3 are presented for the NACA 1-65-050 and NACA 1-50-100 nose-inlet - central-body combinations in figures 16 and 17. At the lowest inlet-velocity ratios for all nose-inlet - central-body combinations, the total-pressure loss across the annulus is high as a result of flow separation from the central-body surface ahead of the inlet. As the inlet-velocity ratio is increased and the back pressure acting on the central-body boundary layer is reduced, the central-body boundary layer attaches and follows the surface of the central body into the inlet. Thus the greater part of the flow enters the inlet with no loss of total pressure for the subsonic Mach numbers and with the very small loss (less than 0.018 $(H_o - p_o)$) sustained through the shock ahead of the inlet for the supersonic Mach numbers. As the inlet-velocity ratio is increased further, the central-body boundary layer becomes thinner and, at still higher inlet-velocity ratios, appreciable losses arise from flow separation from the inner surface of the inlet lip (figs. 16(c) and 17). This flow separation, which may become important at the lower part of the inlet for high angles of attack, can be avoided by the use of a thicker inner-lip fairing.

The average total-pressure-loss coefficient of the flow at the inlet rake station is presented in figures 18 and 19 as a function of inlet-velocity ratio. For some configurations, the spacing of the tubes of the total-pressure rake was not the optimum. The values of total-pressure-loss coefficient may not, therefore, be accurate for conditions where appreciable curvature was indicated for those portions of the curves of figures 16 and 17 which were extrapolated over a relatively large distance to the central-body surface. However, the tube spacing is not believed to have fundamentally altered the shapes of the average total-pressure-loss-coefficient curves.

As shown in figures 18 and 19, for all nose-inlet - central-body combinations at all test Mach numbers, the minimum average total-pressure-loss coefficient was small (less than 0.03 $(H_o - p_o)$). The total-pressure recovery of these subsonic inlets was thus sensibly unimpaired at the supersonic Mach number of 1.2.

A comparison of the curves of figure 18 for a Mach number of 0.8 indicates that, for each configuration, as the inlet-velocity ratio was reduced from the maximum test value, the inlet-velocity ratio at which the total-pressure losses began to rise was approximately the same, but the loss increase was much more abrupt for the conical central bodies B and C. The addition of the parabolic curve to the profile of the conical central bodies ahead of the inlet presumably abrogated the advantages of the wholly conical central body by steepening the adverse pressure gradient just ahead of the inlet as a result of the induced velocities over the curved parabolic surface.

The central-body boundary layer may have been laminar at the point of separation for the models of these tests. A lower minimum inlet-velocity ratio for unseparated central-body flow might result therefore in a full-scale installation if the Reynolds number and surface roughness were such as to induce boundary-layer transition ahead of the separation point.

The dashed curves of figures 18 and 19 were interpolated from unpublished data gathered for NACA 1-series spinners in the investigation reported in reference 2. These curves were interpolated from total-pressure measurements just inside the inlet for two spinners of the proportions of the two elliptical central bodies of the present tests. Since there is little difference in NACA 1-series or elliptical profiles when applied to given central-body proportions, no significant differences are expected in the aerodynamic characteristics of central bodies with either of these profiles. Although the dashed curves of figures 18 and 19 were obtained from measurements with an NACA 1-85-050 and an NACA 1-55-050 nose inlet, respectively, reference 2 has shown that, when the distance from the central-body surface to the inlet lip is 0.075D or greater, central-body flow-separation characteristics are

essentially independent of the proportions of the nose inlet. The ticks shown on the curves denote the minimum inlet-velocity ratio for unseparated spinner flow as specified in reference 2.

No large differences were found in the average total-pressure-loss curves of the elliptical central bodies of the present tests and the NACA 1-series spinners of reference 2 for widely different Mach numbers (figs. 18(a) and 19). The disagreement shown in figure 19 between the data at 0.13 Mach number and the data point at the lowest inlet-velocity ratio at 0.4 Mach number is probably due principally to the difference in Reynolds number. The minimum inlet-velocity ratio for which the total-pressure losses remained near minimum levels decreased appreciably, however, for the conical central bodies B and C, when the Mach number was increased from 0.8 to 1.2 (figs. 18(b) and 18(c)).

From figure 18(a), it is indicated that the low-speed measurement of the minimum inlet-velocity ratio for unseparated central-body flow given in reference 2 is directly applicable at Mach numbers extending up to 1.2. The validity of the low-speed minimum inlet-velocity ratio for higher Mach numbers is not as reliably established in figure 19, but if there is a difference in the low-speed minimum inlet-velocity ratio indicated by the tick and the inlet-velocity ratio of the total-pressure-loss increase at higher Mach numbers, the difference cannot be large.

CONCLUSIONS

The following conclusions are drawn from an investigation of three NACA 1-series nose inlets and four nose-inlet - central-body combinations at subsonic Mach numbers and at a supersonic Mach number of 1.2:

1. For the nose inlets, the external pressure-drag coefficient at a Mach number of 1.2 was consecutively lower for the nose inlets of greater length ratio. The external pressure-drag coefficient for the longest nose inlet was in the range of pressure-drag coefficient for two solid noses of fineness ratio 2.4 and 6.0.

2. For Mach numbers below the Mach number of the supercritical drag rise, extrapolation of the test data indicated that the external drag of the nose inlets was little affected by the addition of central bodies at or slightly below the minimum inlet-velocity ratio for unseparated central-body flow.

3. The addition of central bodies to the nose inlets led to no appreciable effects on either the Mach number of the supercritical drag

rise or, for inlet-velocity ratios high enough to avoid a pressure peak at the inlet lip, on the critical Mach number.

4. The total-pressure recovery of the inlets tested, which were of a subsonic type, was sensibly unimpaired at a Mach number of 1.2.

5. A comparison of the inlet total-pressure losses for an elliptical and two conical-type central bodies showed that the minimum inlet-velocity ratio below which the inlet total-pressure losses began to rise was approximately the same, but the loss increase was much more abrupt for the conical-type central bodies.

6. Low-speed measurements of the minimum inlet-velocity ratio for unseparated central-body flow appear to be applicable for Mach numbers extending up to 1.2.

Langley Aeronautical Laboratory,
National Advisory Committee for Aeronautics,
Langley Field, Va., January 6, 1950.

REFERENCES

1. Baals, Donald D., Smith, Norman F., and Wright, John B.: The Development and Application of High-Critical-Speed Nose Inlets. NACA Rep. 920, 1948. (Supersedes NACA ACR L5F30a.)

2. Nichols, Mark R., and Keith, Arvid L., Jr.: Investigation of a Systematic Group of NACA 1-Series Cowlings With and Without Spinners. NACA Rep. 950, 1949. (Supersedes NACA RM L8A15.)

3. Pendley, Robert E., and Smith, Norman F.: An Investigation of the Characteristics of Three NACA 1-Series Nose Inlets at Subcritical and Supercritical Mach Numbers. NACA RM L8L06, 1949.

4. Ferri, Antonio, and Nucci, Louis M.: Preliminary Investigation of a New Type of Supersonic Inlet. NACA Rep. 1104, 1952. (Supersedes NACA TN 2286.)

5. Matthews, Clarence W.: Pressure Distributions over a Wing-Fuselage Model at Mach Numbers of 0.4 to 0.99 and at 1.2. NACA RM L8H06, 1948.

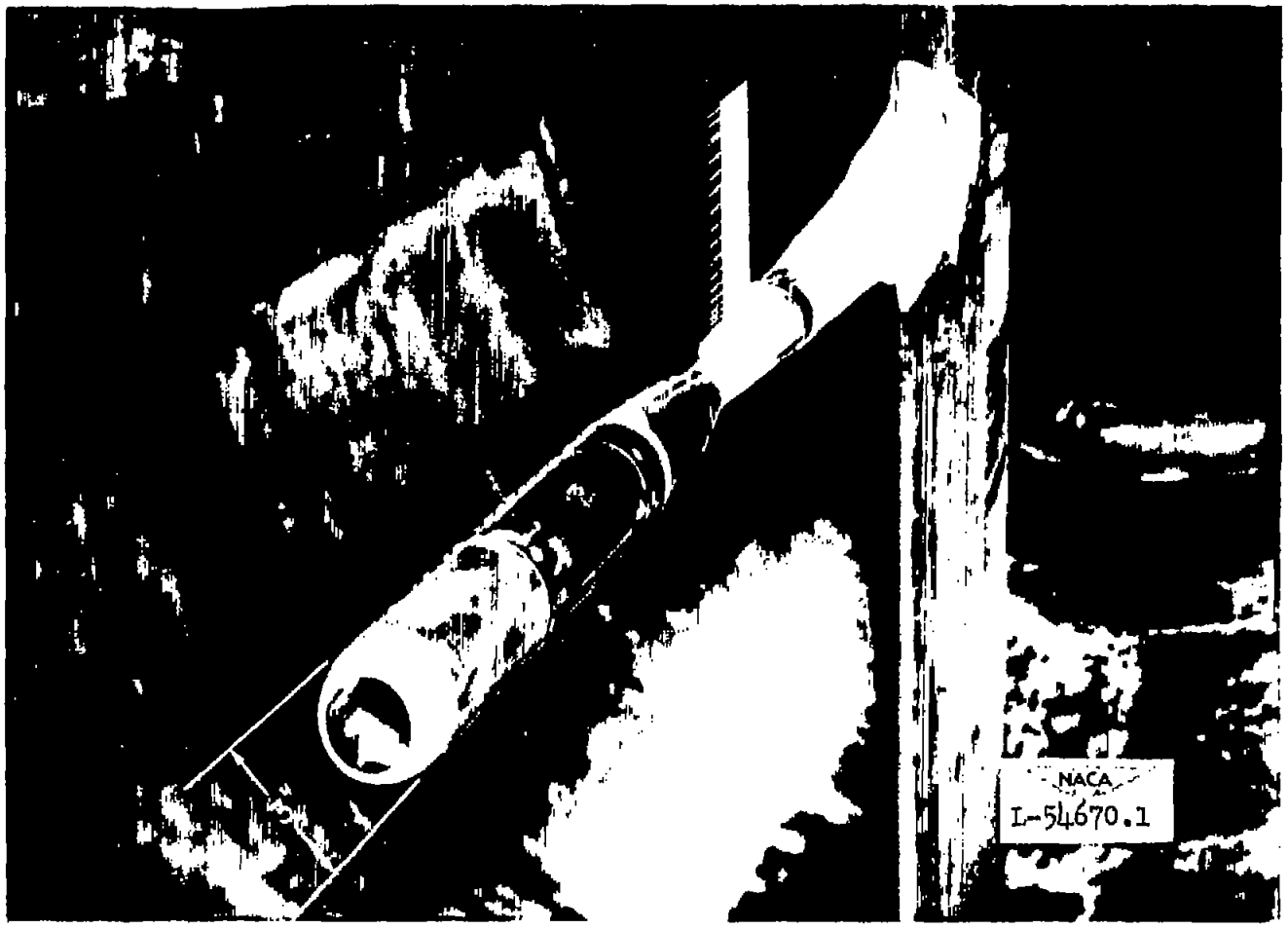

(a) Model and wake-survey rake in subsonic test section.

Figure 1.- Model installation in Langley 8-foot high-speed tunnel.

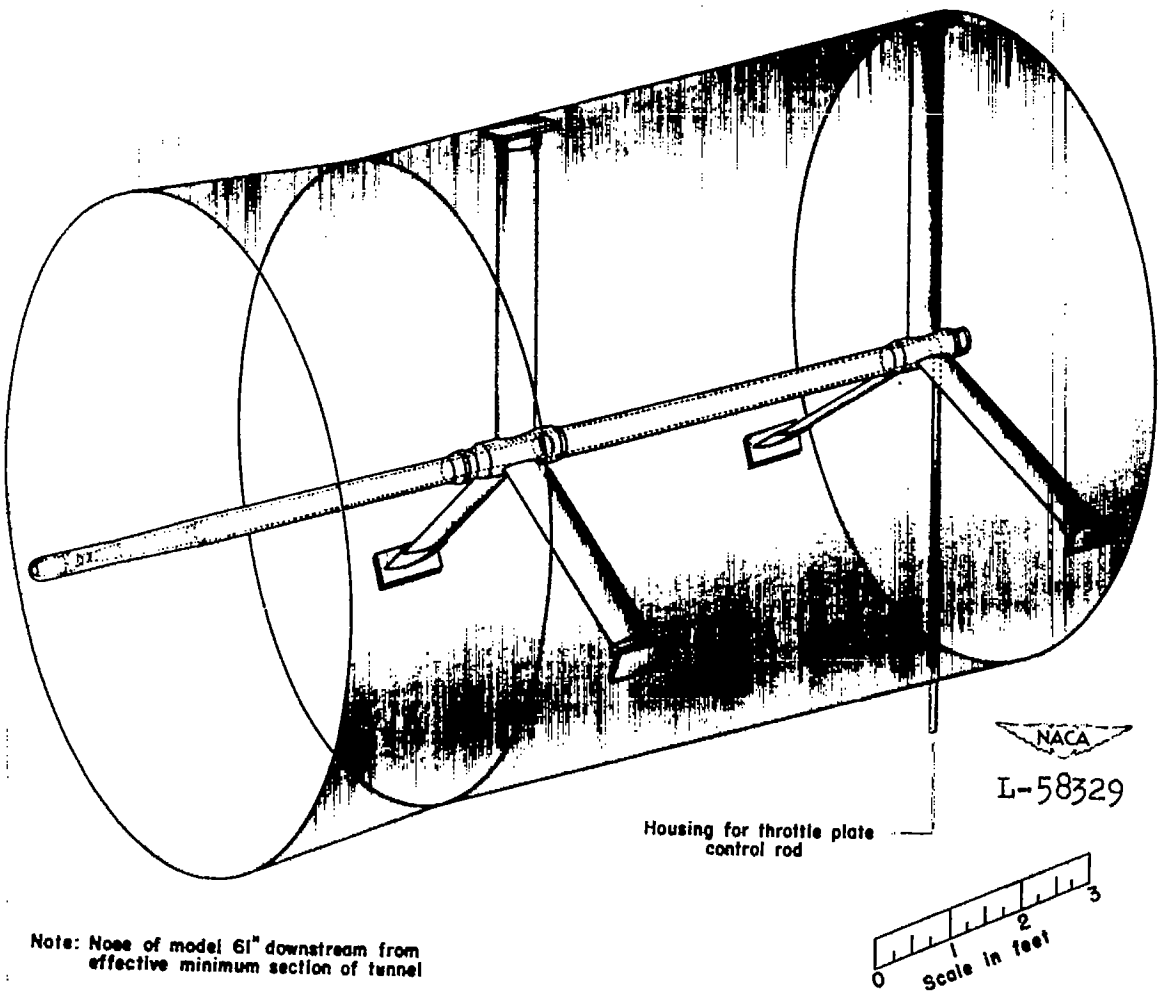

(b) Model in supersonic test section.

Figure 1.- Concluded.

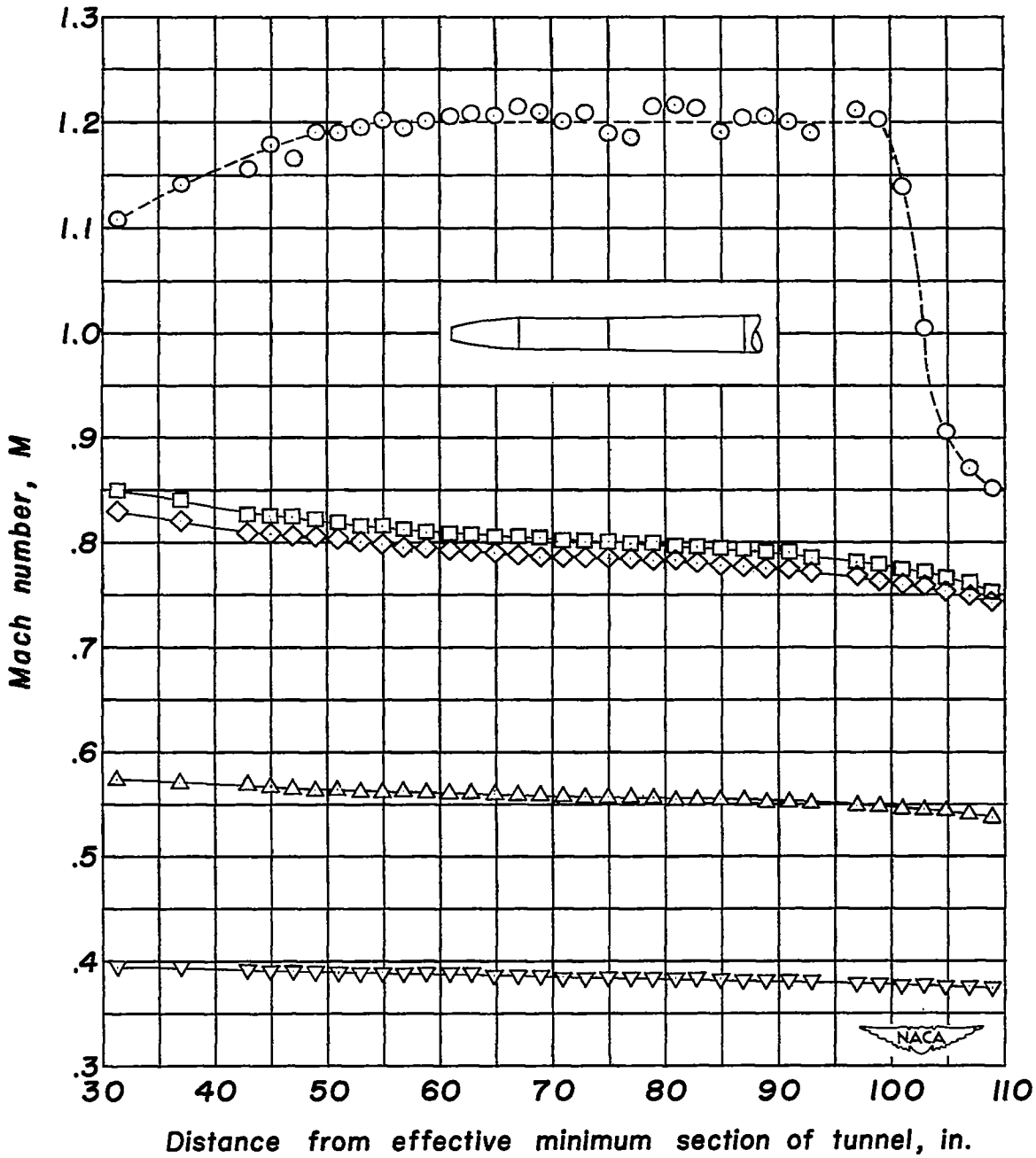

Figure 2.- Mach number distributions along the tunnel center line in the supersonic test section. Tunnel empty.

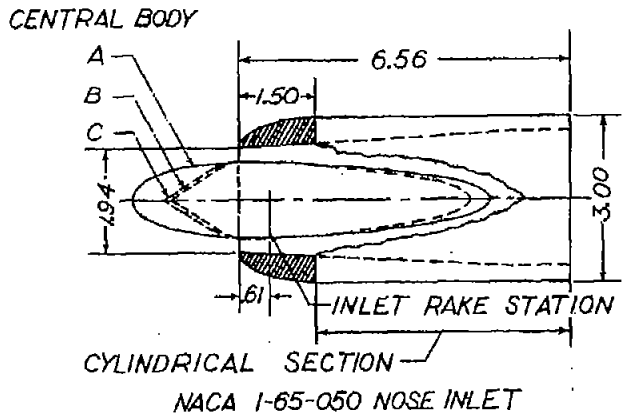

NACA 1-65-050 NOSE INLET

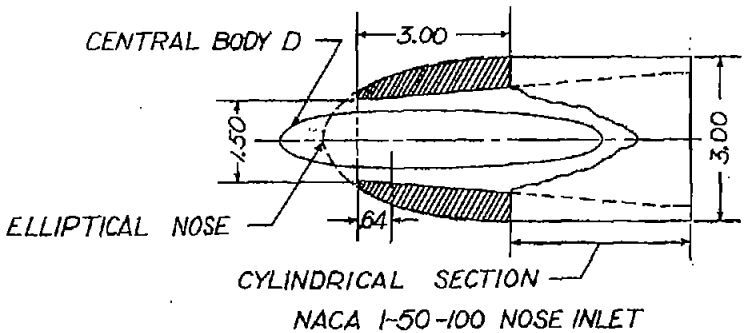

NACA 1-50-100 NOSE INLET

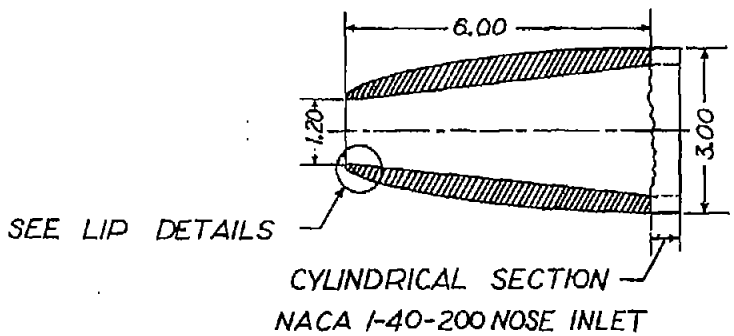

NACA 1-40-200 NOSE INLET

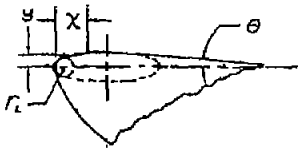

NACA 1-65-050		NACA 1-50-100		NACA 1-40-200	
x	y	x	y	x	y
.009	.018	.018	.019	.036	.026
.015	.021	.030	.021	.060	.031
.030	.024	.060	.026	.120	.034
.045	.027	.090	.028	.180	.031
.060	.029	.120	.029		
.075	.031	.150	.026		
.090	.032				
.110	.033				
.150	.030				
r_i = 0.019		r_i = 0.018		r_i = 0.022	
θ = 3.0°		θ = 4.5°		θ = 6.0°	

NOSE INLET LIP DETAILS

Figure 3.- Model combinations tested. All dimensions are in inches.

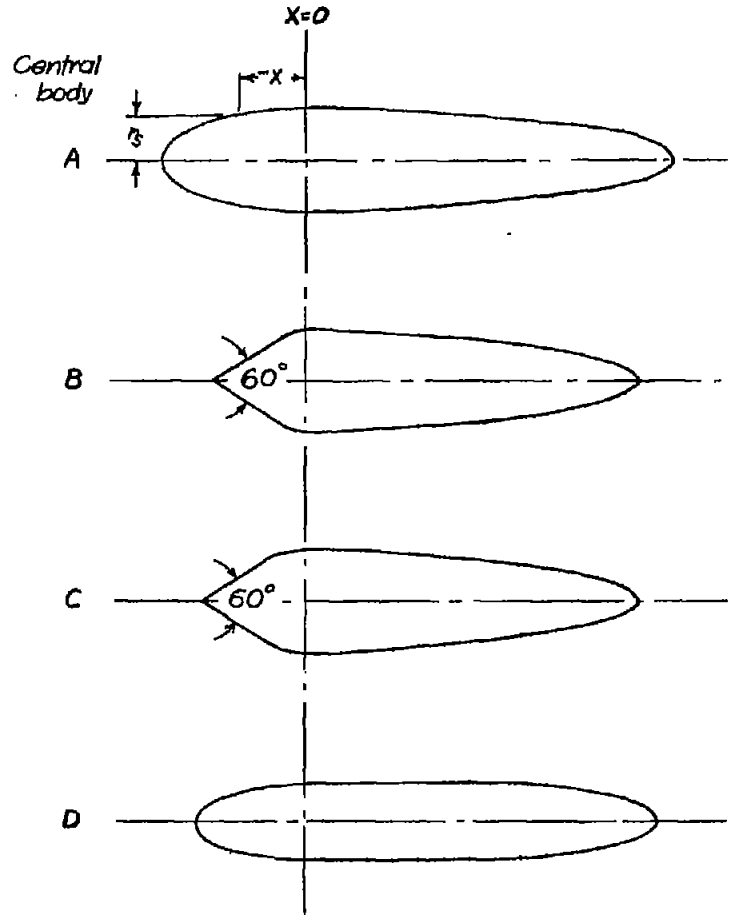

Central-body A Ordinates	
x, in.	r_s, in.
-2.025	0
-2.000	.106
-1.900	.234
-1.800	.309
-1.600	.414
-1.400	.487
-1.200	.543
-1.000	.587
-.800	.620
-.600	.645
-.400	.662
-.200	.672
0	.675
.187	.675
.687	.658
1.187	.634

Central-body B Ordinates	
x, in.	r_s, in.
-1.322	0
-.283	.603
-.234	.629
-.176	.654
-.117	.672
-.059	.682
0	.686
.110	.686
.200	.683
.400	.674
.600	.664
.900	.649
1.200	.631

Central-body C Ordinates	
x, in.	r_s, in.
-1.466	0
-.566	.522
-.468	.574
-.351	.622
-.234	.658
-.117	.679
0	.686
.200	.683
.400	.674
.600	.664
.900	.649
1.200	.631

Central-body D Ordinates	
x, in.	r_s, in.
-1.500	0
-1.375	.200
-1.250	.276
-1.000	.373
-.750	.433
-.500	.471
-.250	.493
0	.500
.187	.500
.500	.513
1.000	.521
1.500	.521
2.000	.520

Figure 4.- Central-body ordinates.

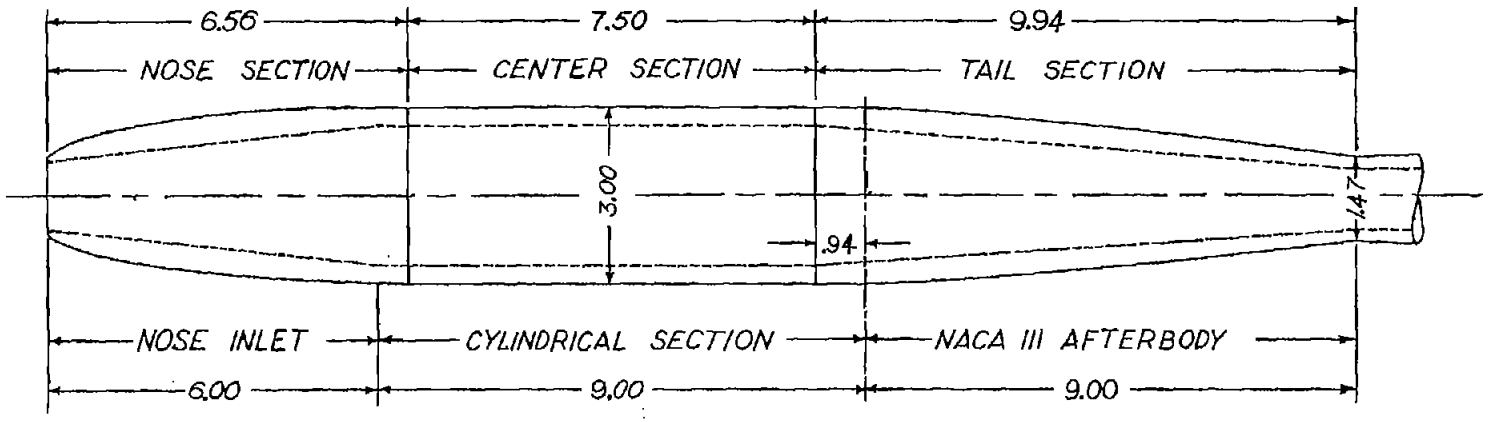

(a) Mounting system in subsonic test section.

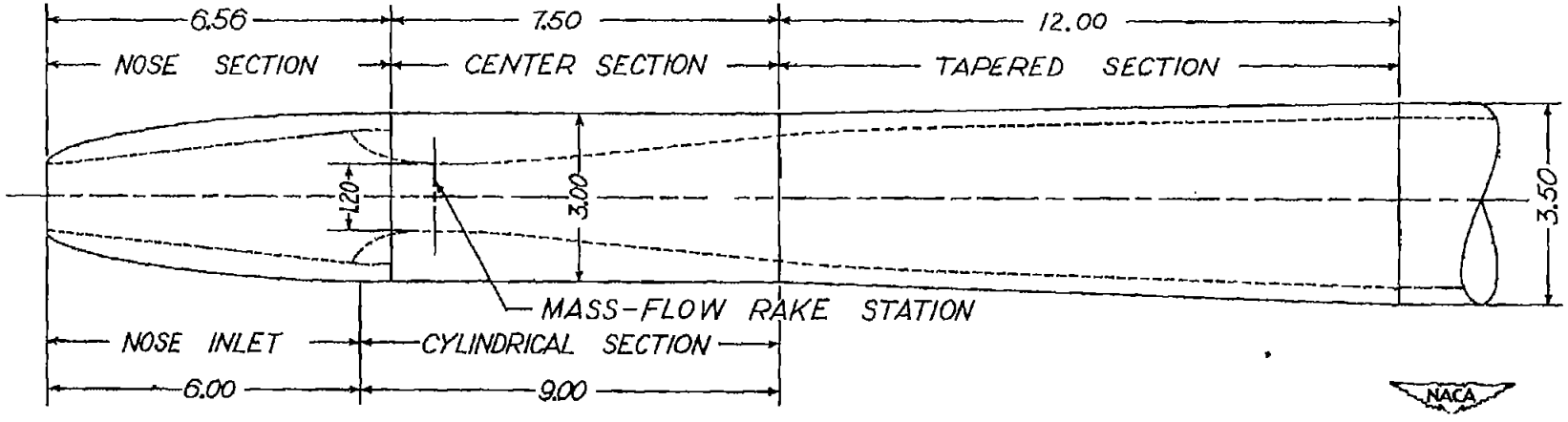

(b) Mounting system in supersonic test section.

Figure 5.- Model mounting systems. (Model shown is NACA 1-40-200 nose inlet.) All dimensions are in inches.

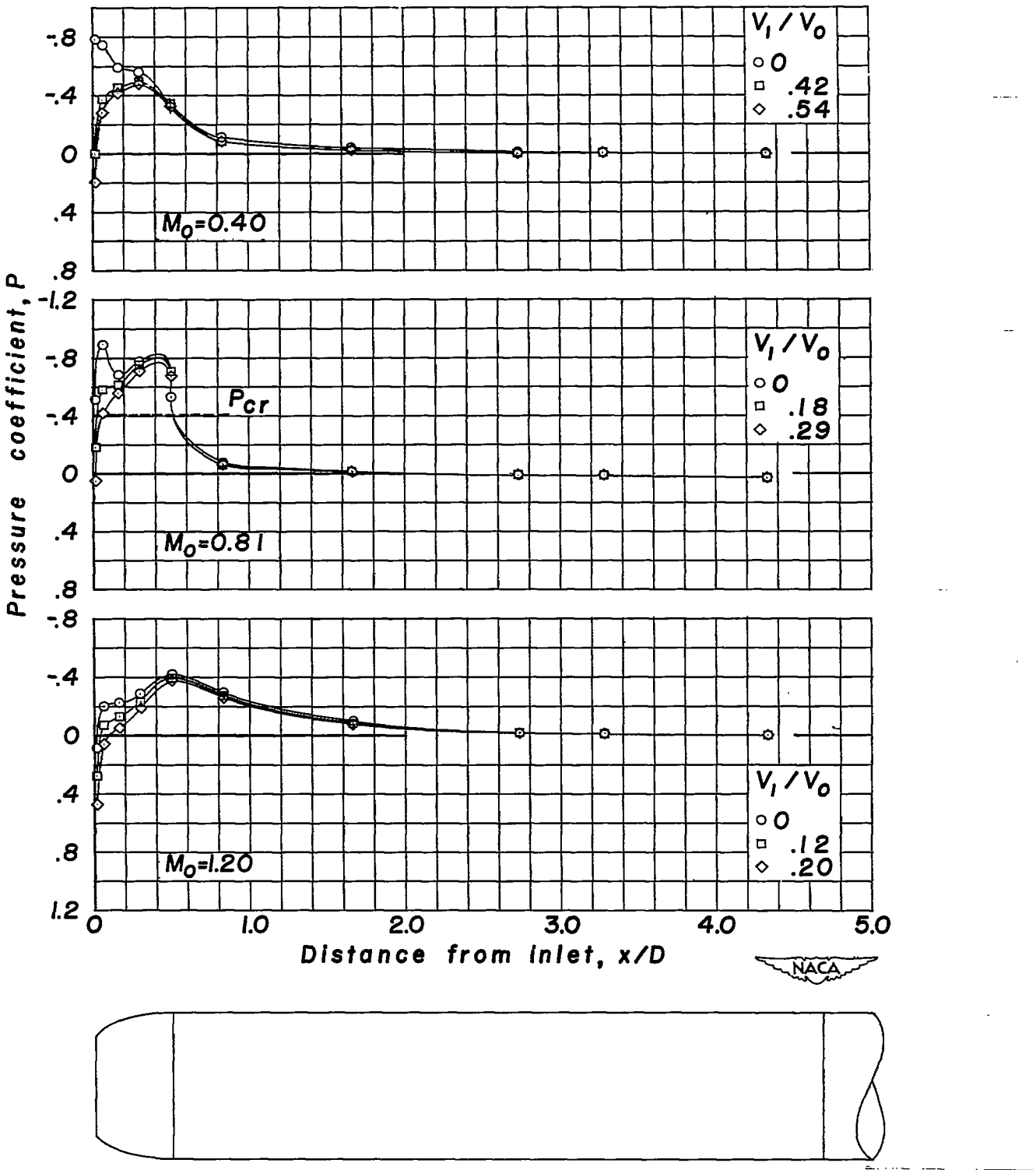

(a) NACA 1-65-050 nose inlet.

Figure 6.- Surface pressure distributions. $\alpha = 0^\circ$.

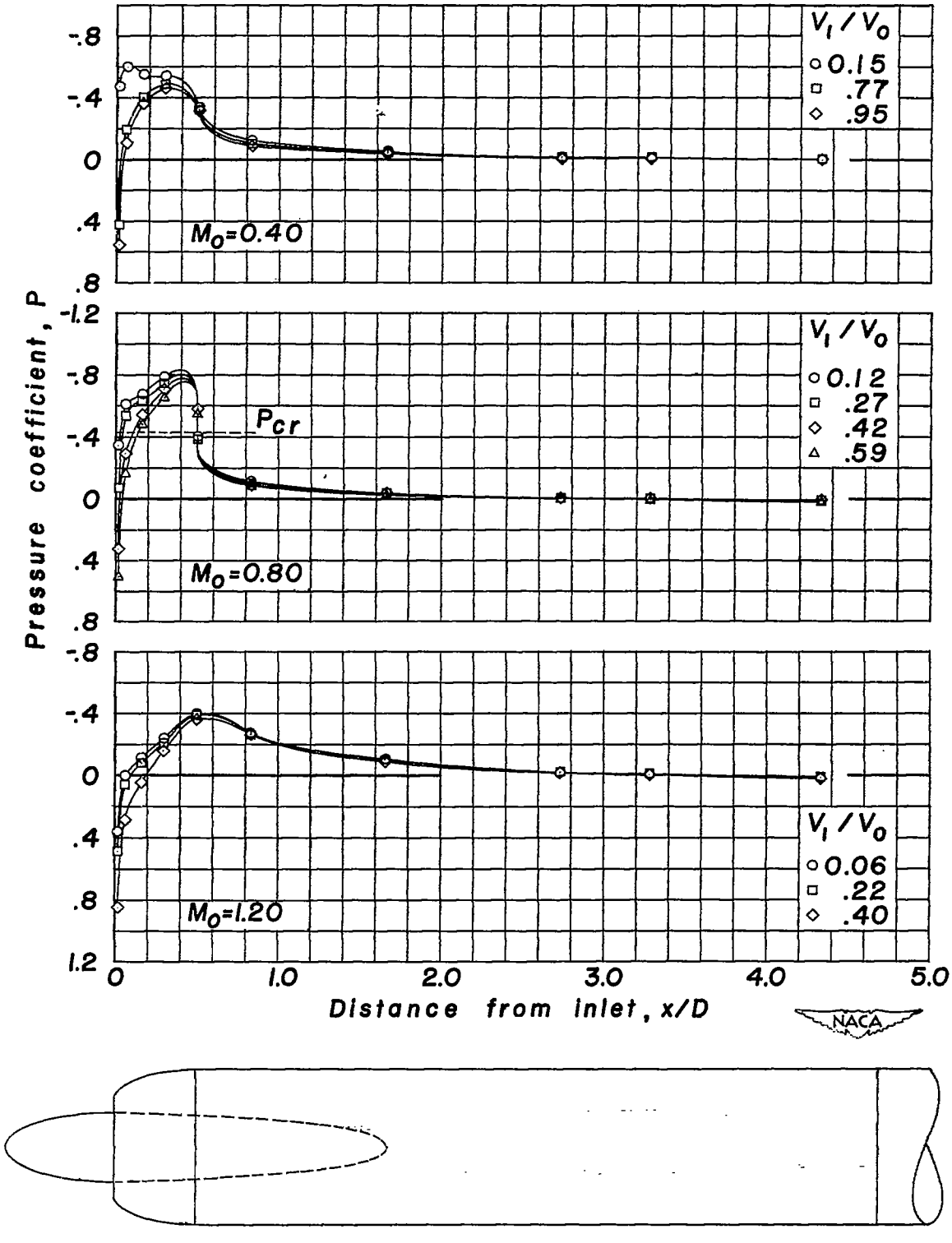

(b) NACA 1-65-050 nose inlet with central body A.

Figure 6.- Continued.

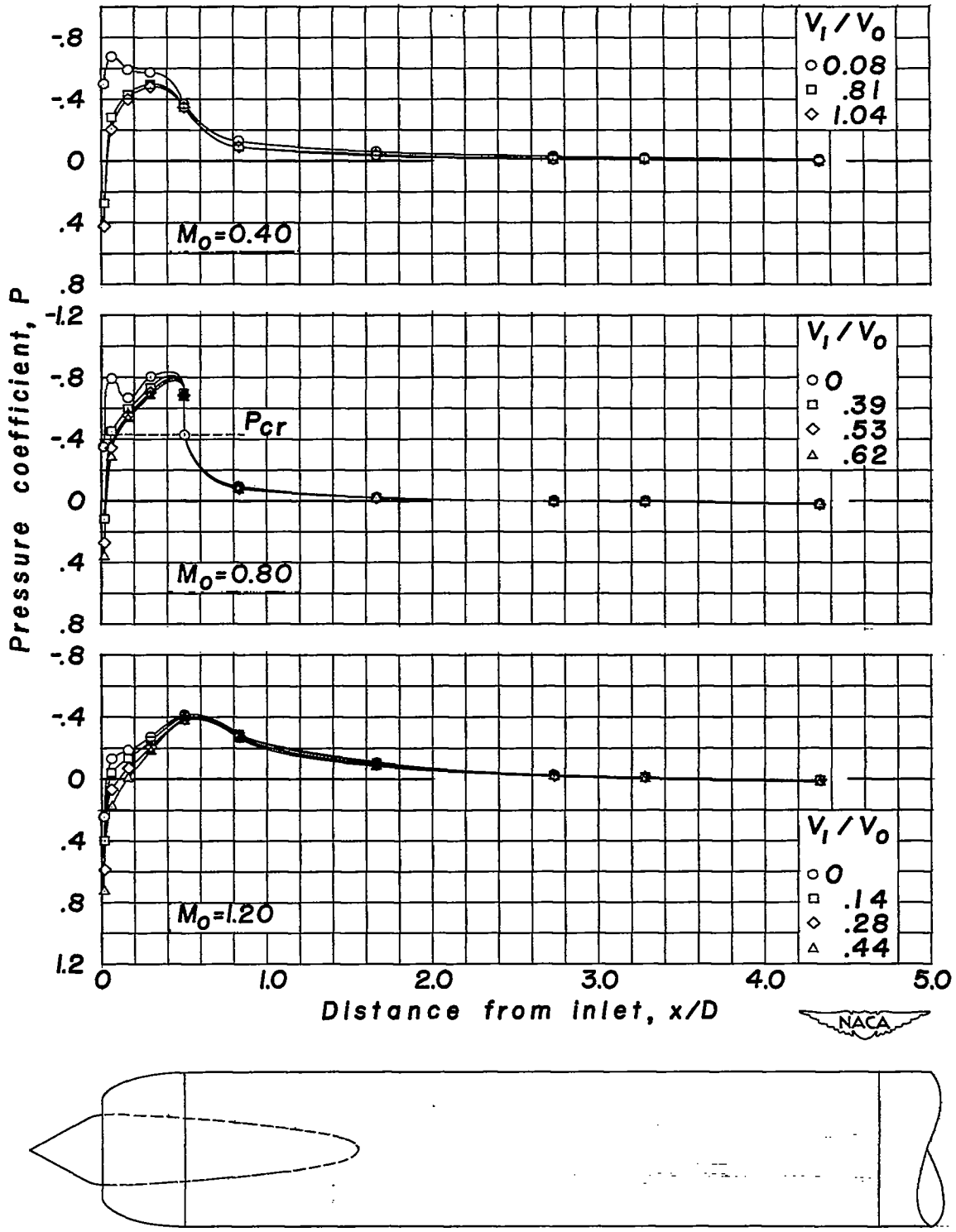

(c) NACA 1-65-050 nose inlet with central body B.

Figure 6.- Continued.

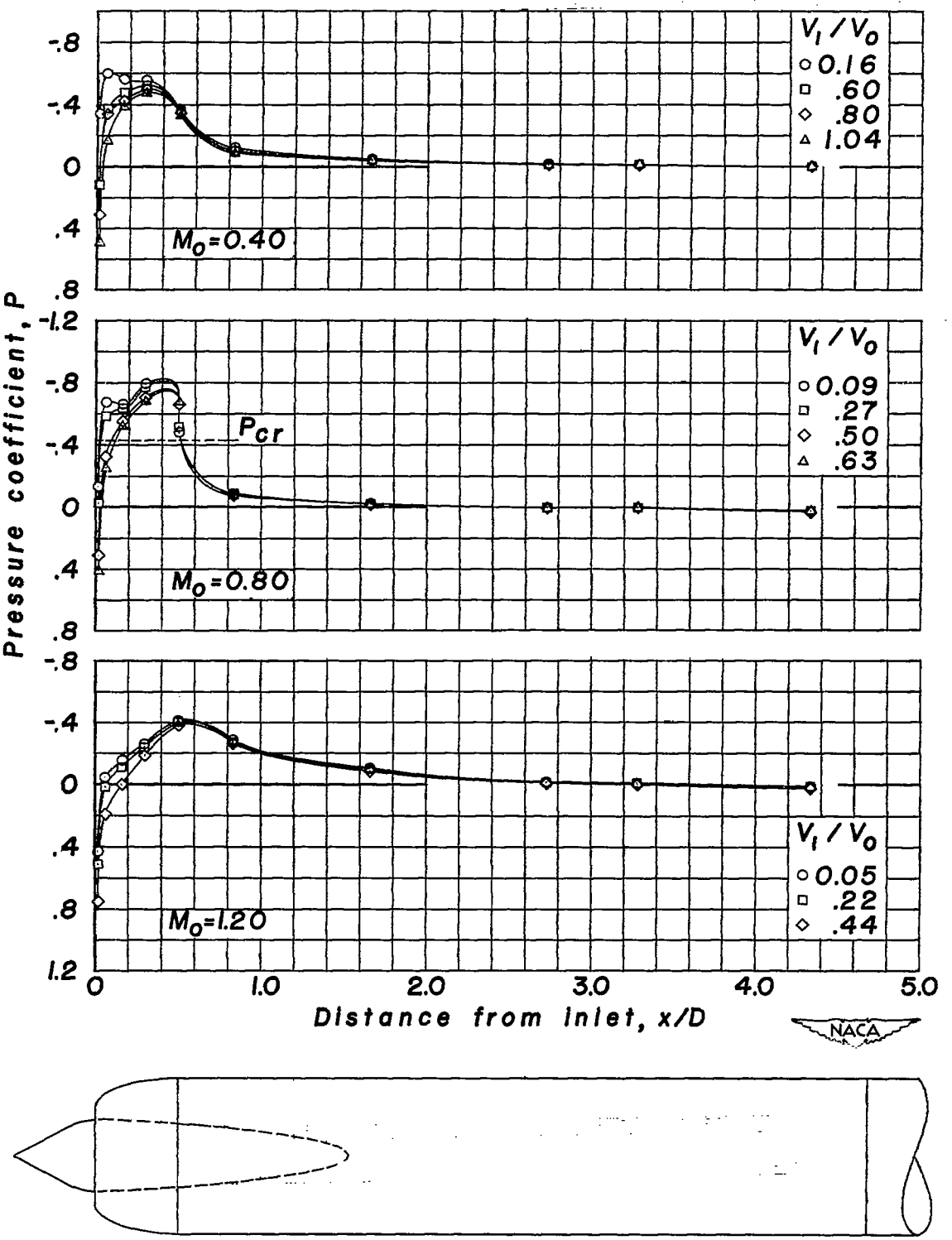

(d) NACA 1-65-050 nose inlet with central body C.

Figure 6.- Continued.

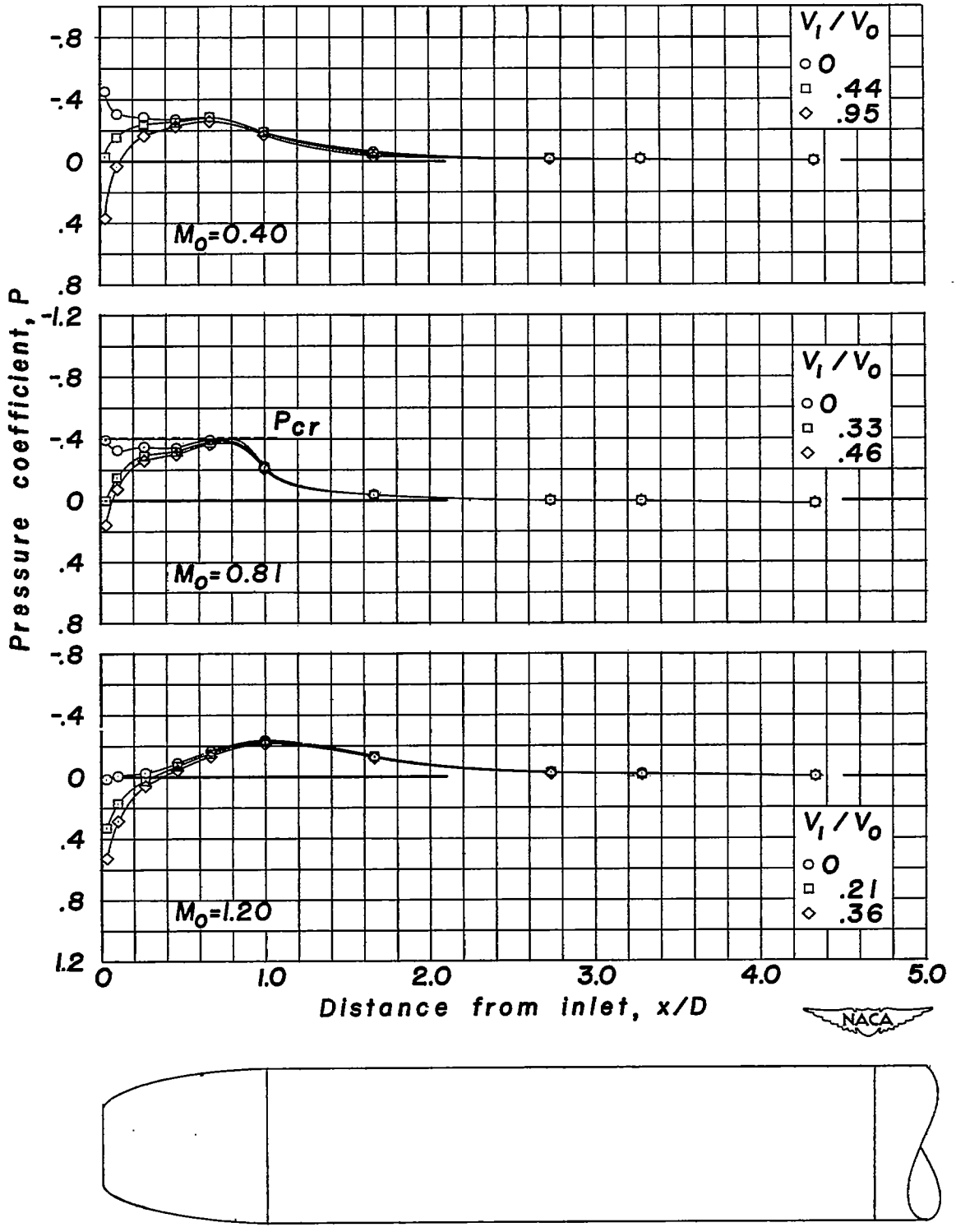

(e) NACA 1-50-100 nose inlet.

Figure 6.- Continued.

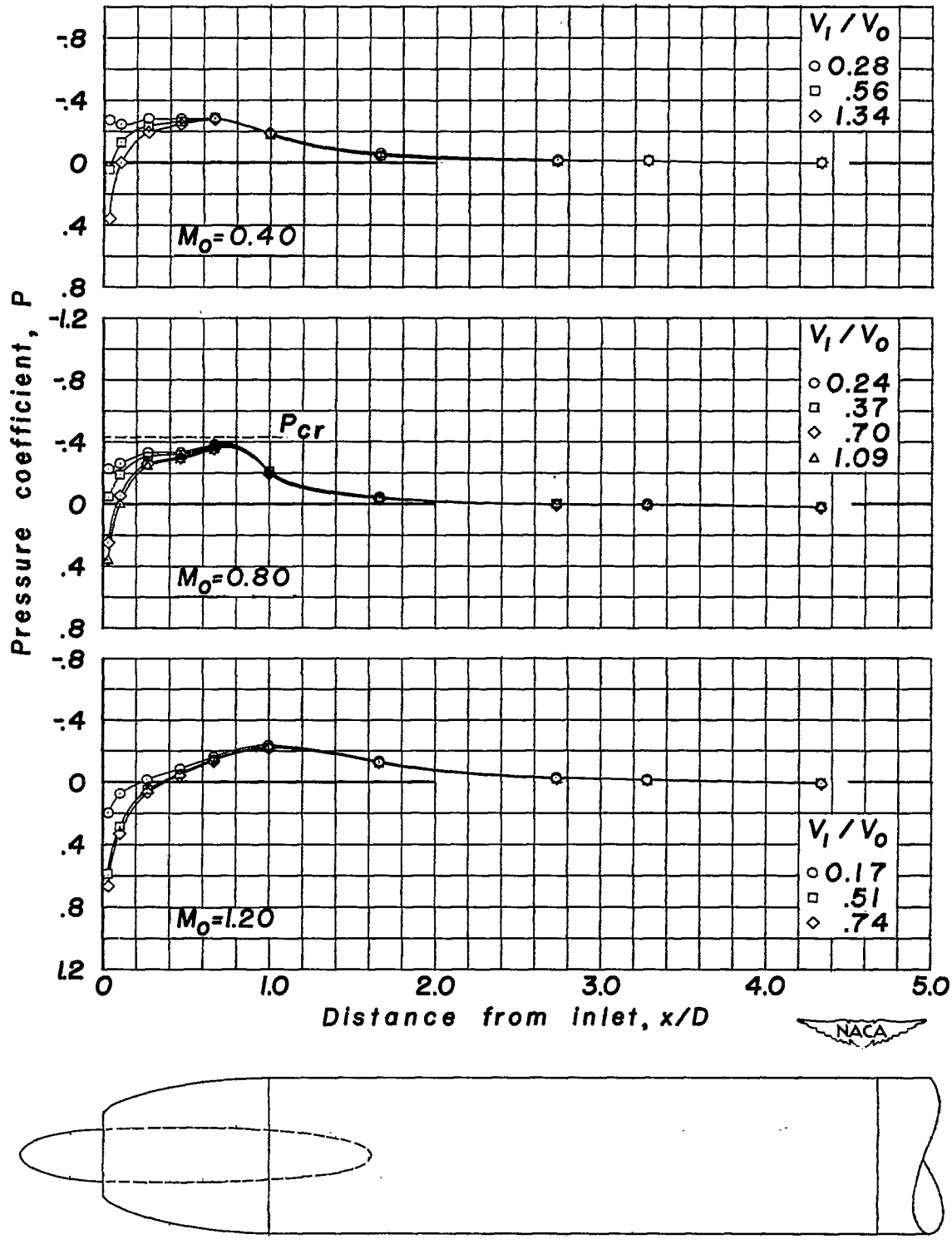

(f) NACA 1-50-100 nose inlet with central body D.

Figure 6.- Continued.

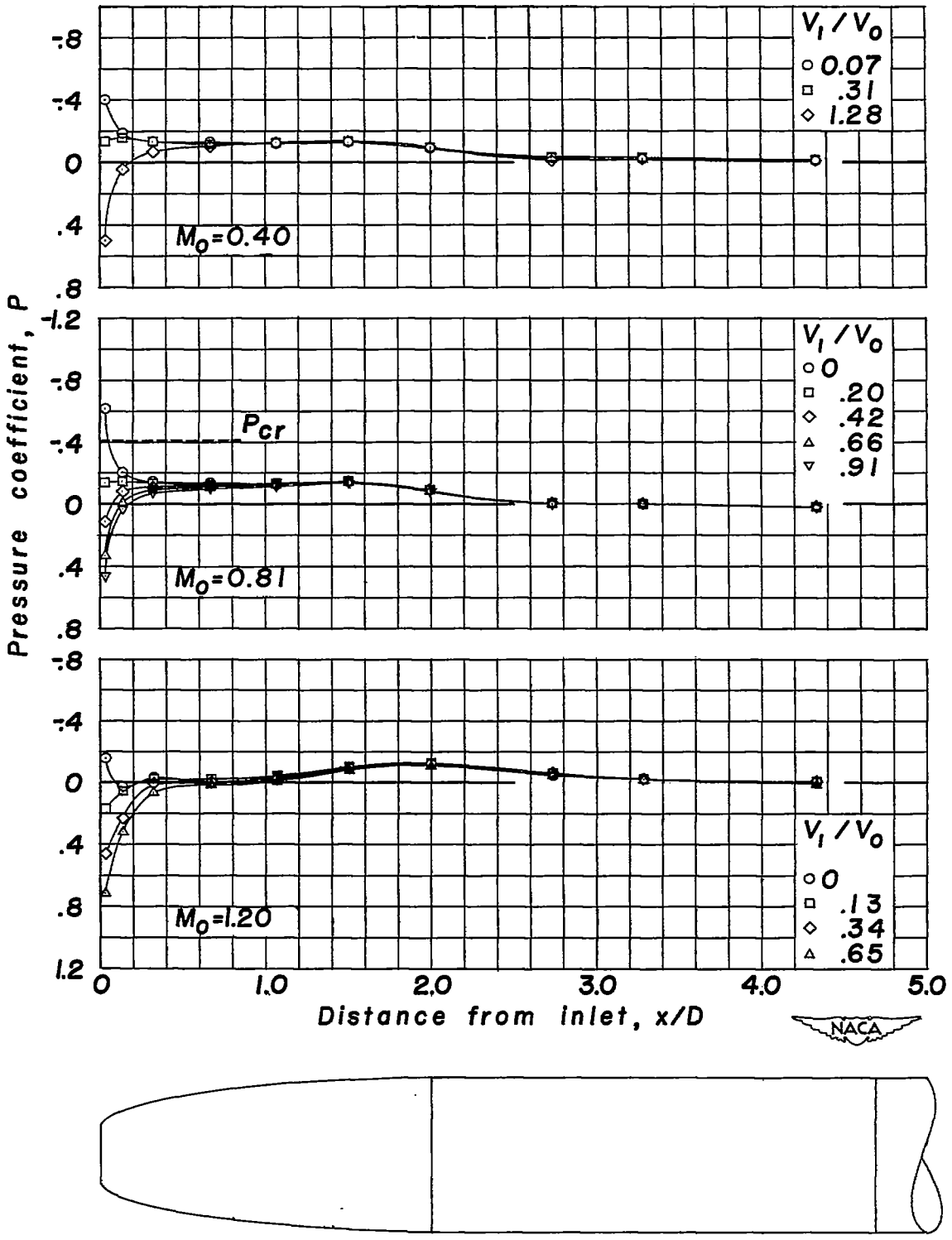

(g) NACA 1-40-200 nose inlet.

Figure 6.- Concluded.

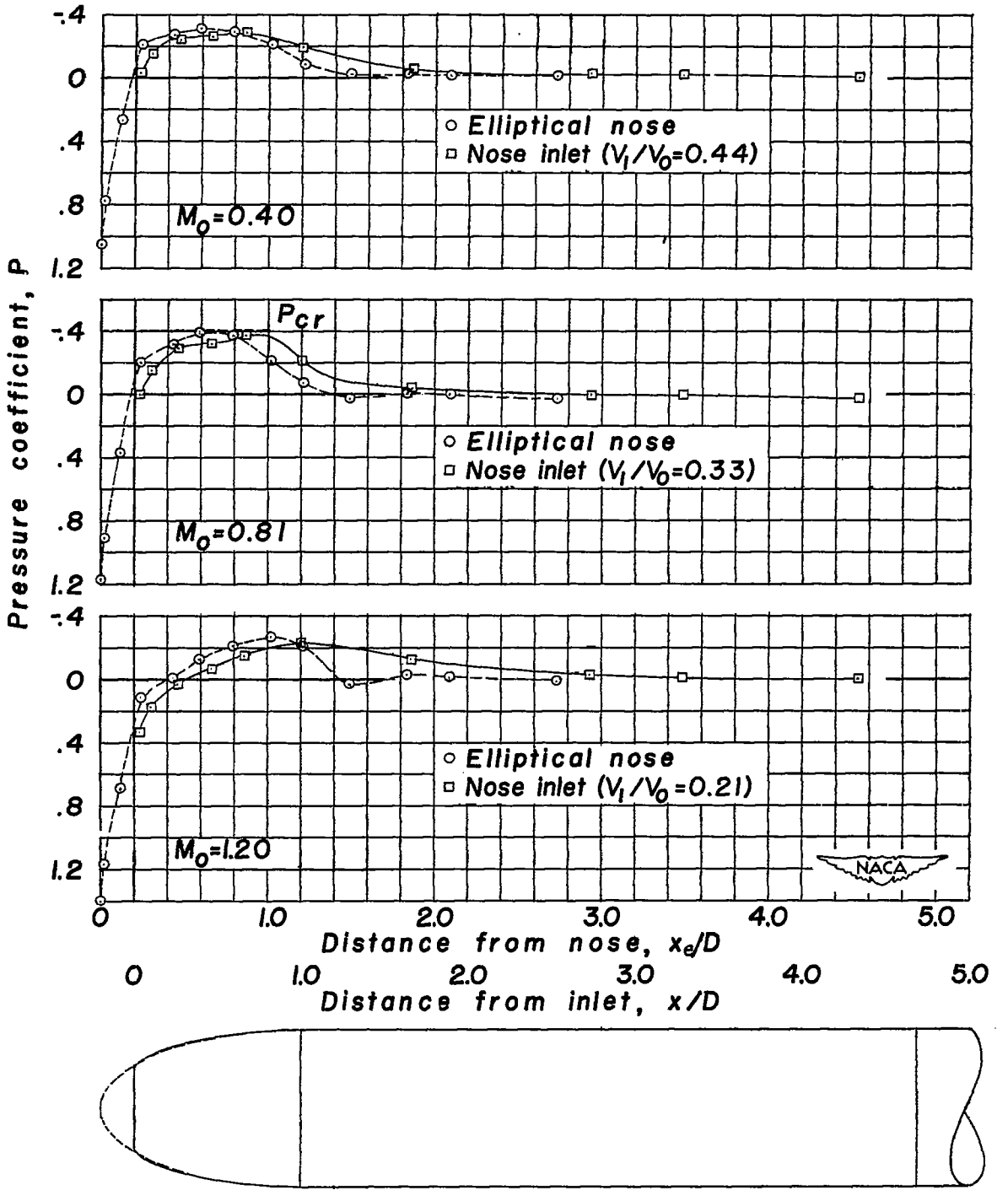

Figure 7.- Comparison of surface pressure distributions of elliptical nose and NACA 1-50-100 nose inlet. $\alpha = 0^\circ$.

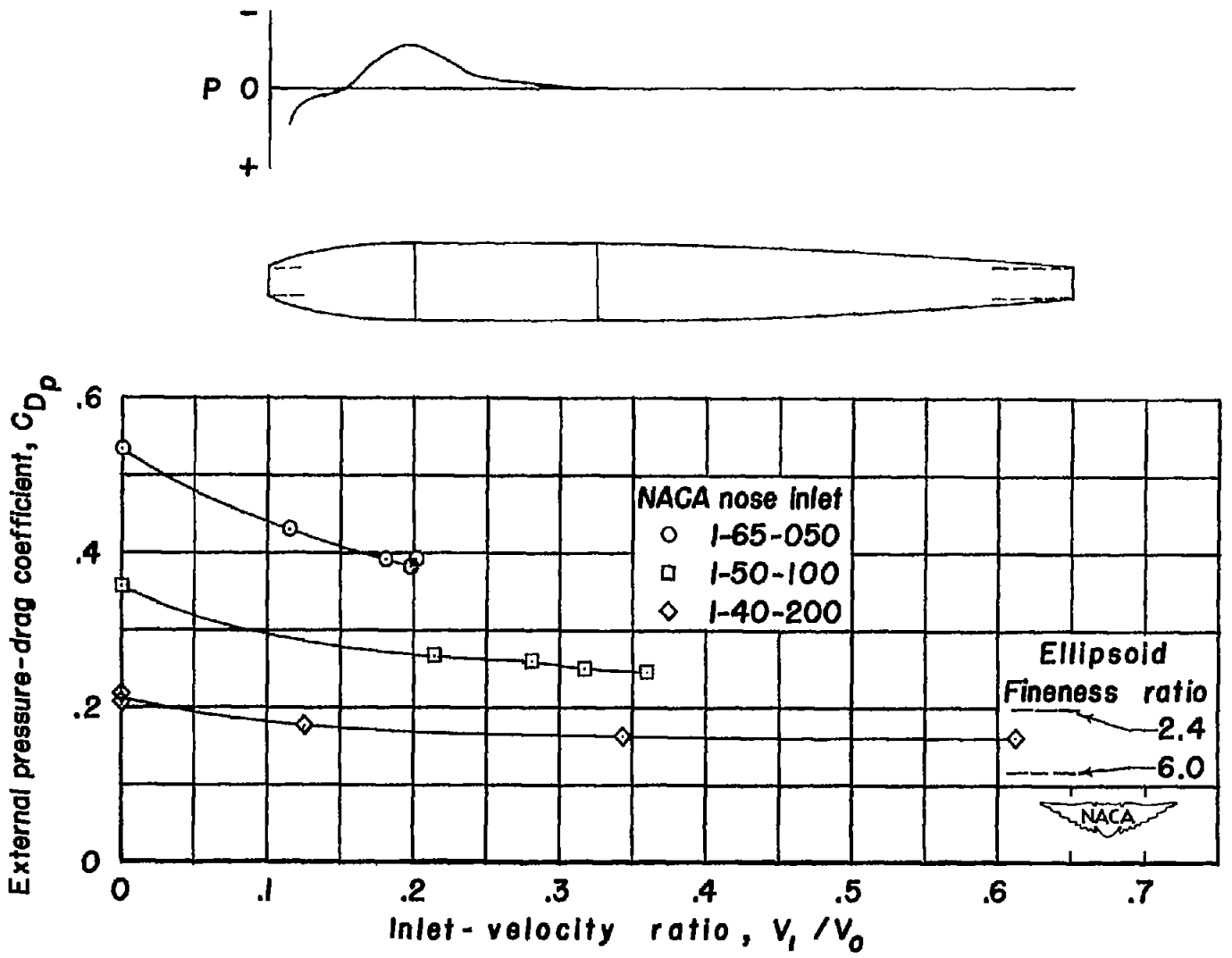

Figure 8.- Comparison of external pressure-drag coefficients. $M_0 = 1.20$; $\alpha = 0^\circ$.

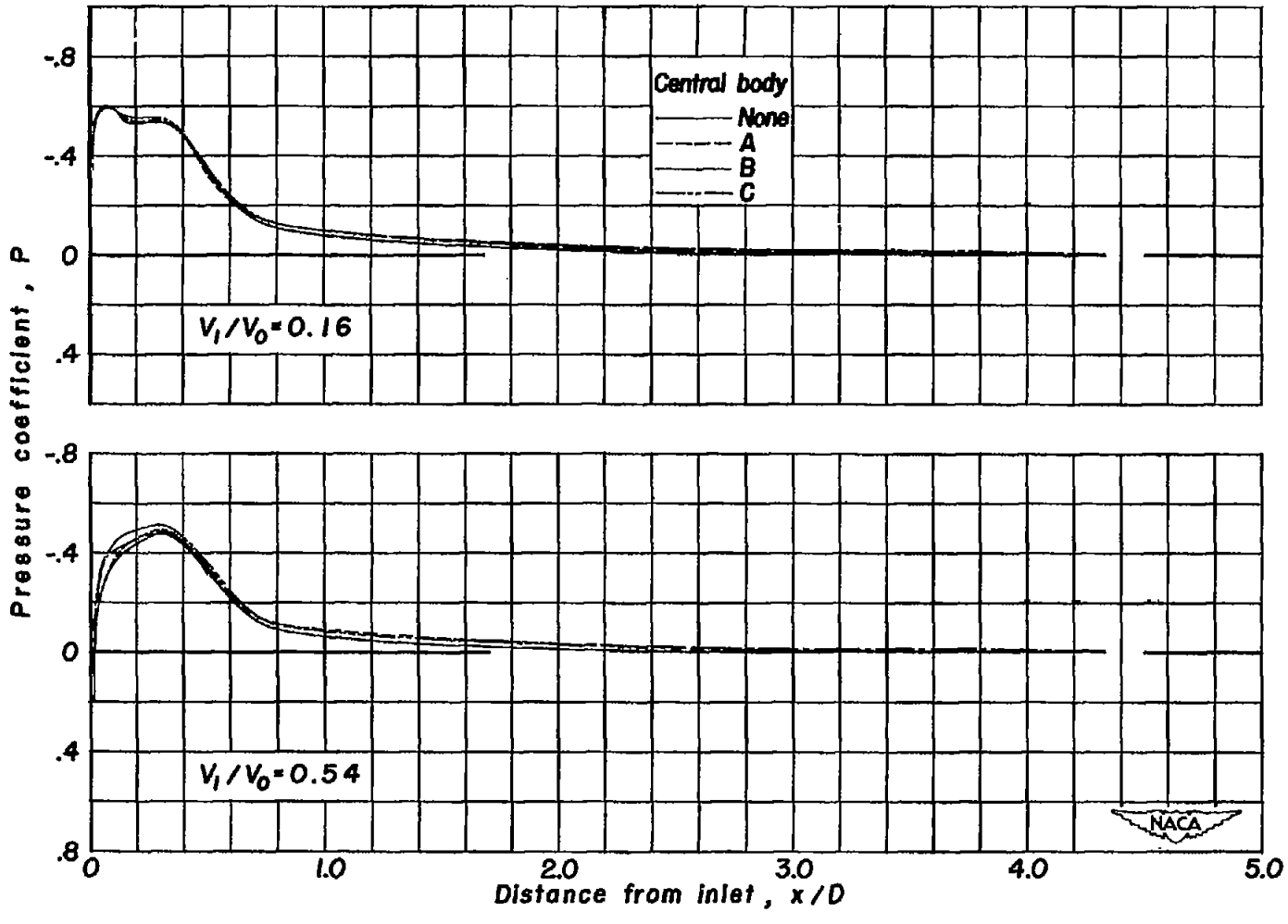

(a) $M_o = 0.40$.

Figure 9.- Effect of central bodies on surface pressure distributions of NACA 1-65-050 nose inlet. $\alpha = 0^o$.

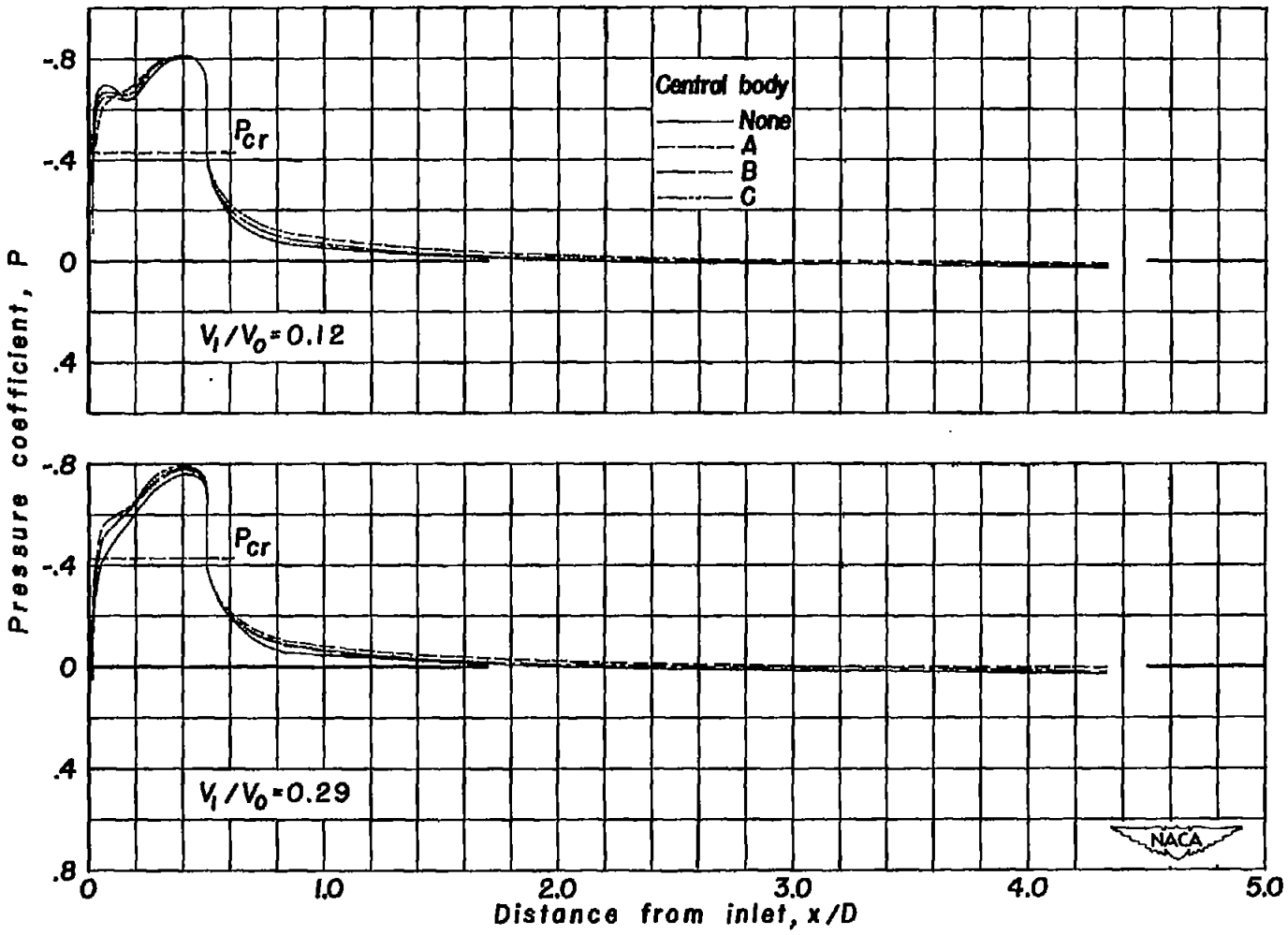

(b) $M_o \approx 0.80$.

Figure 9.- Continued.

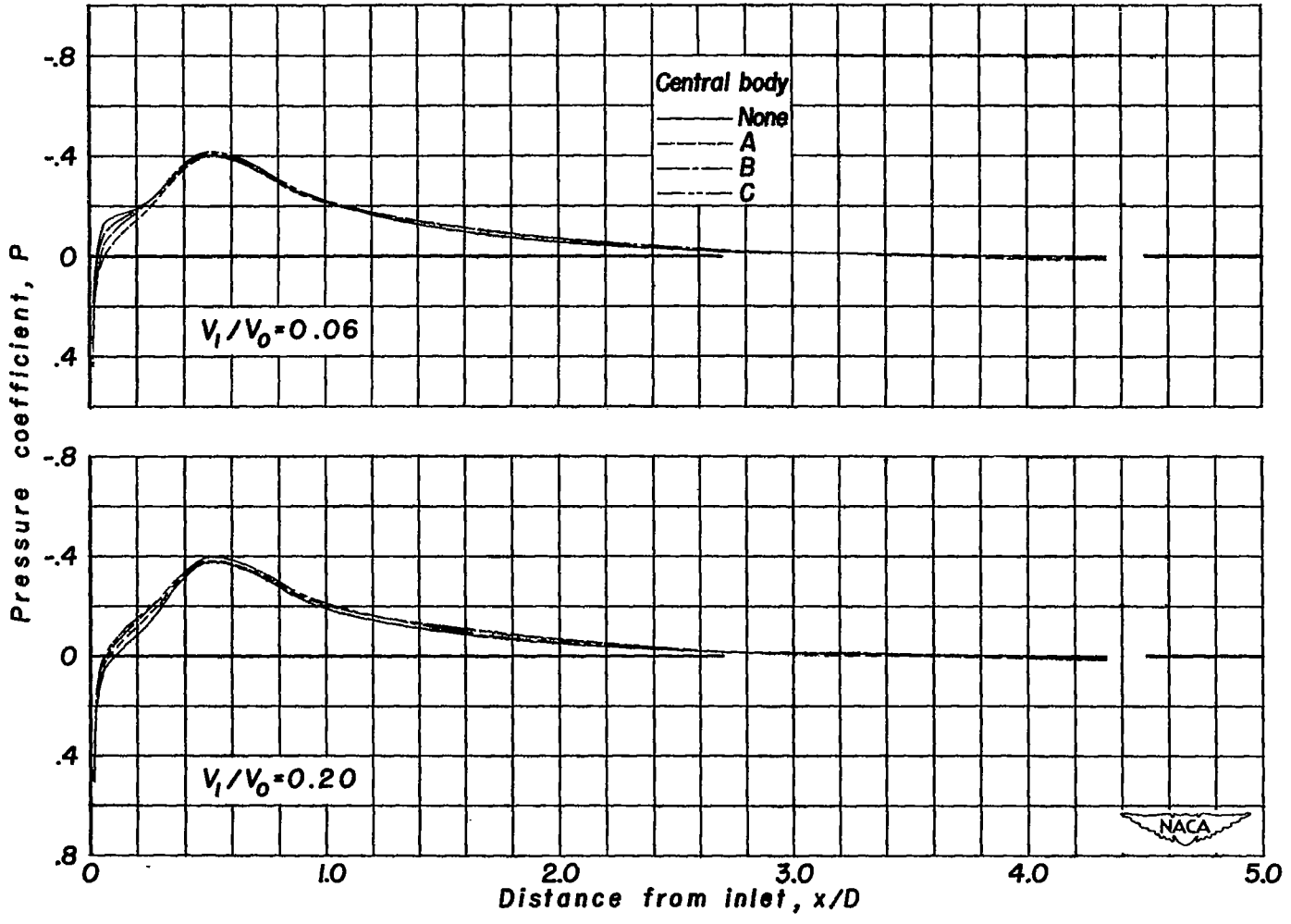

(c) $M_0 = 1.20$.

Figure 9.- Concluded.

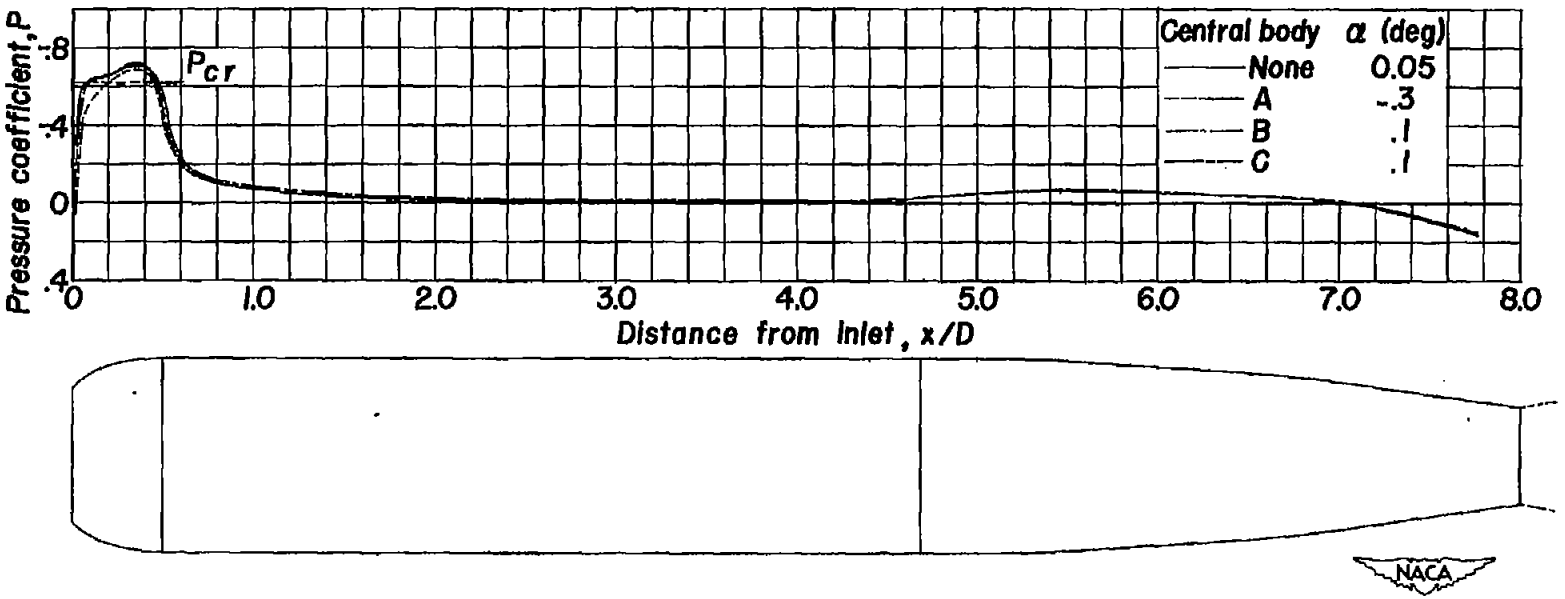

Figure 10.- Effect of central bodies on surface pressure distribution of NACA 1-65-050 nose inlet near M_{cr}. $M_o \approx 0.74$; $\frac{V_1}{V_o} = 0.18$.

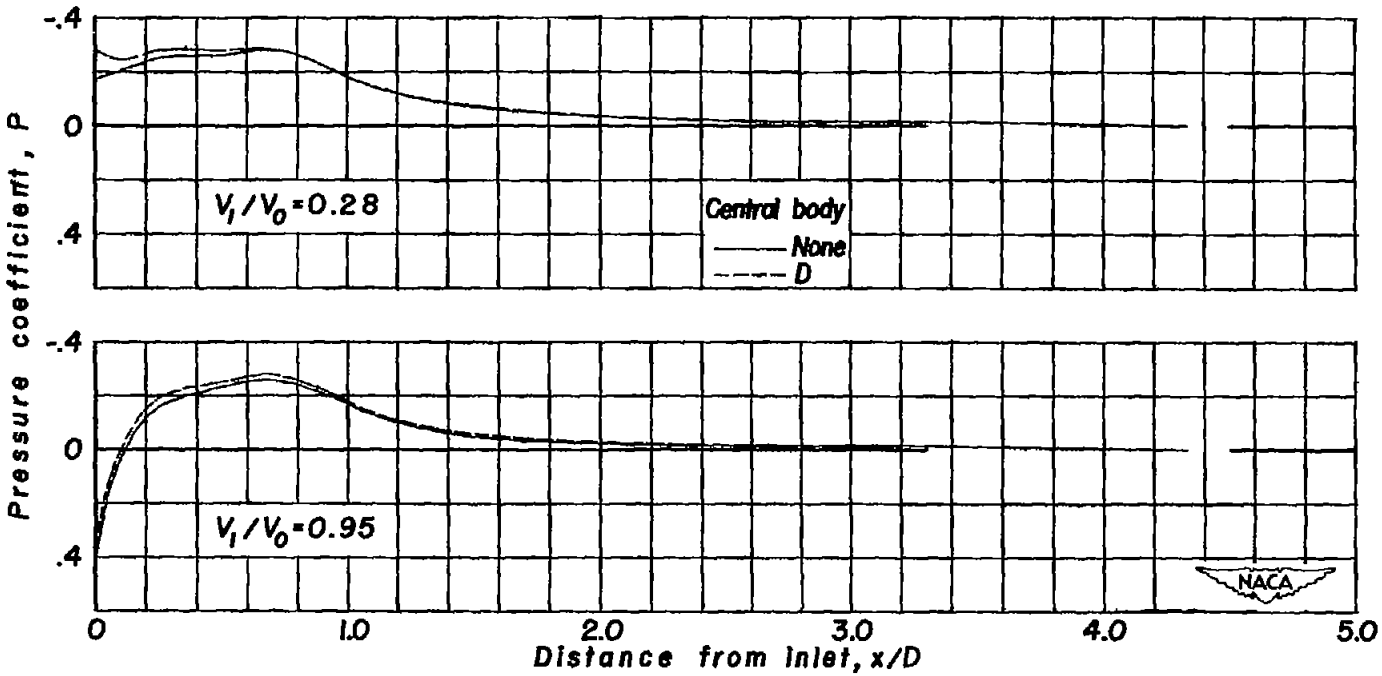

(a) $M_o = 0.40$.

Figure 11.- Effect of central body on surface pressure distributions of NACA 1-50-100 nose inlet. $\alpha = 0^o$.

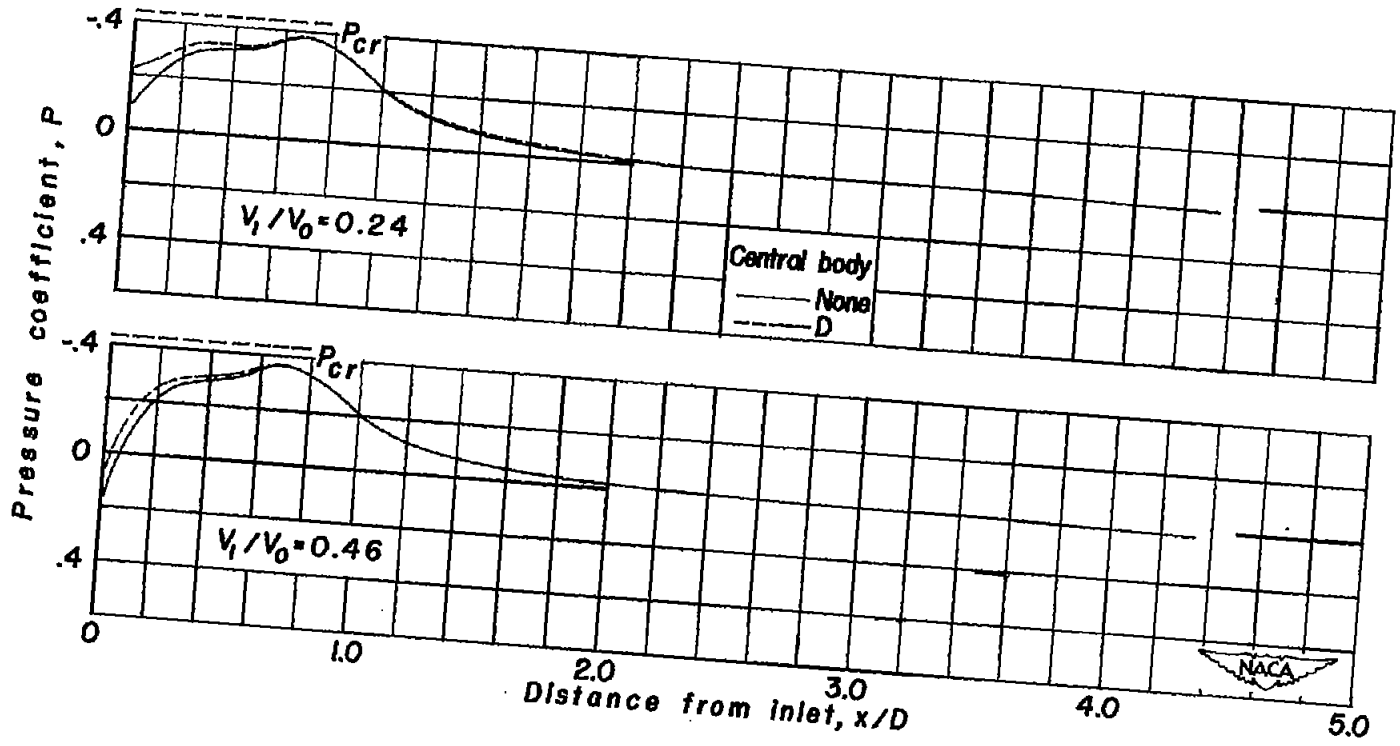

(b) $M_0 \approx 0.80$.

Figure 11.- Continued.

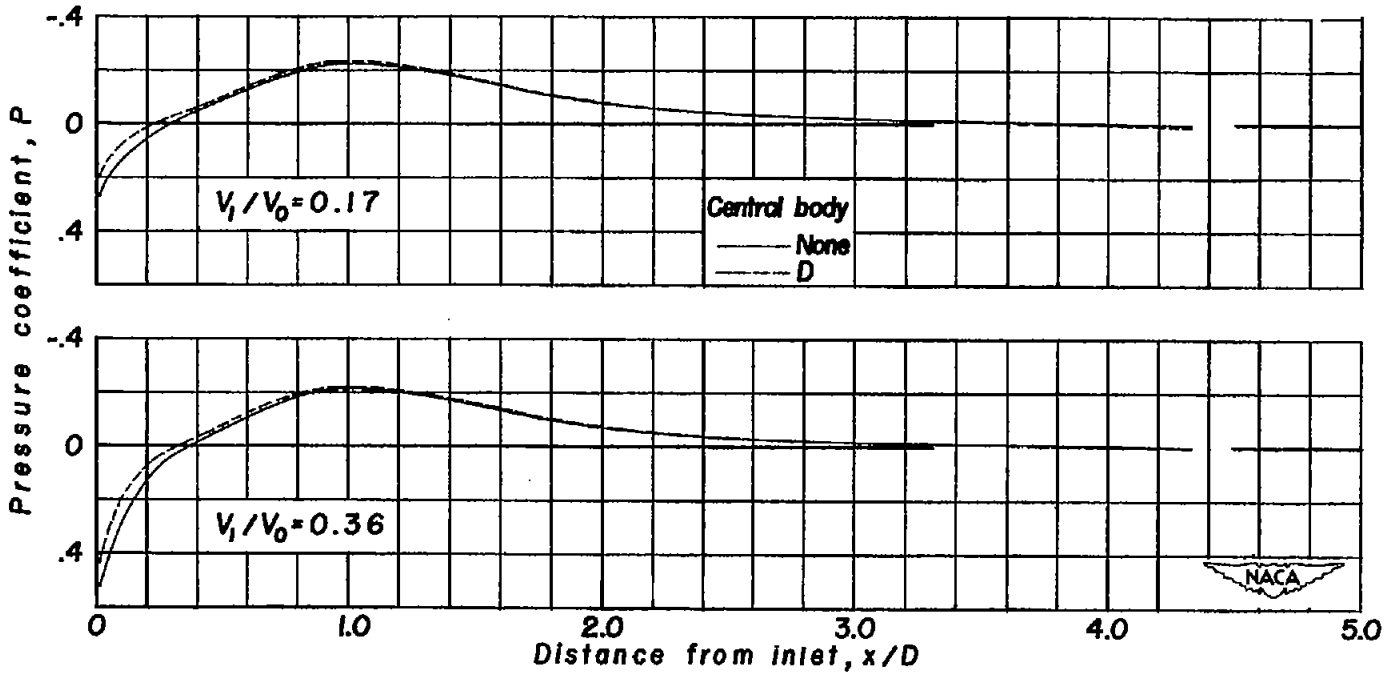

(c) $M_0 = 1.20$.

Figure 11.- Concluded.

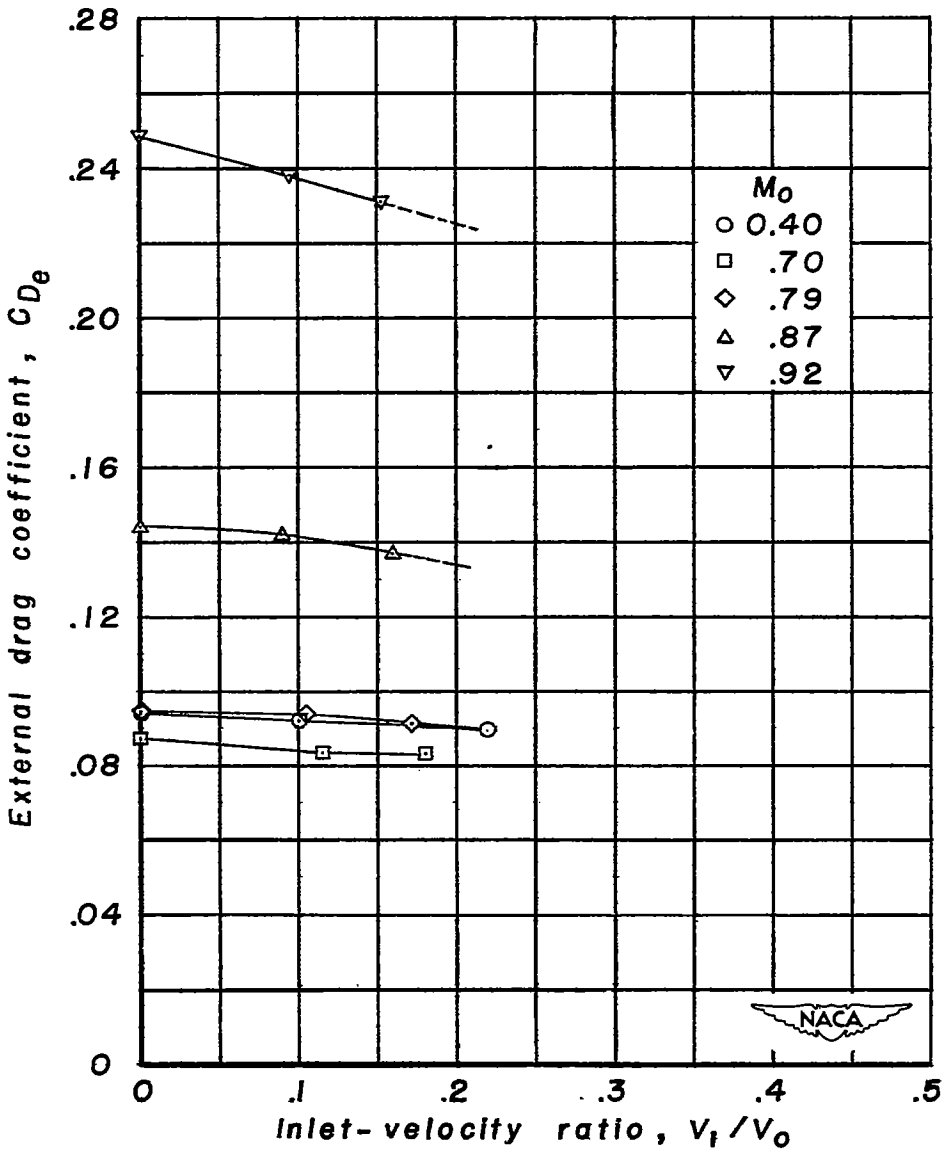

(a) No central body; $\alpha = 0.05^{\circ}$.

Figure 12.- Variation of external drag coefficient with inlet-velocity ratio. NACA 1-65-050 nose inlet with and without central bodies.

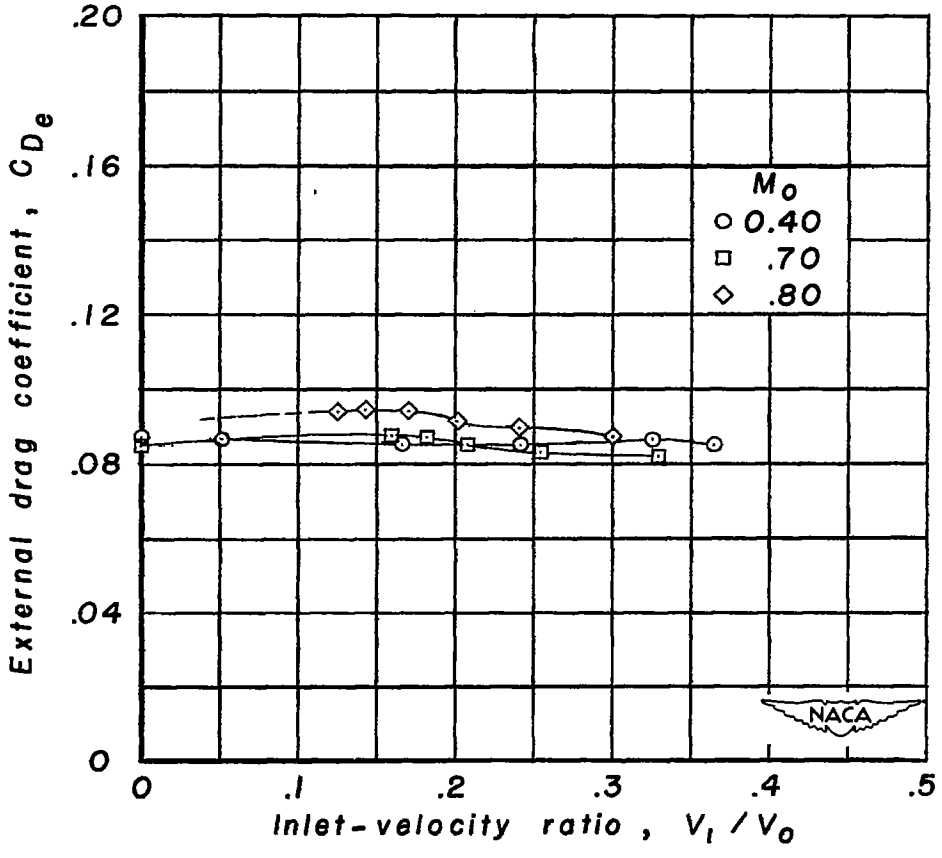

(b) Central body A; $\alpha = -0.3°$.

Figure 12.- Continued.

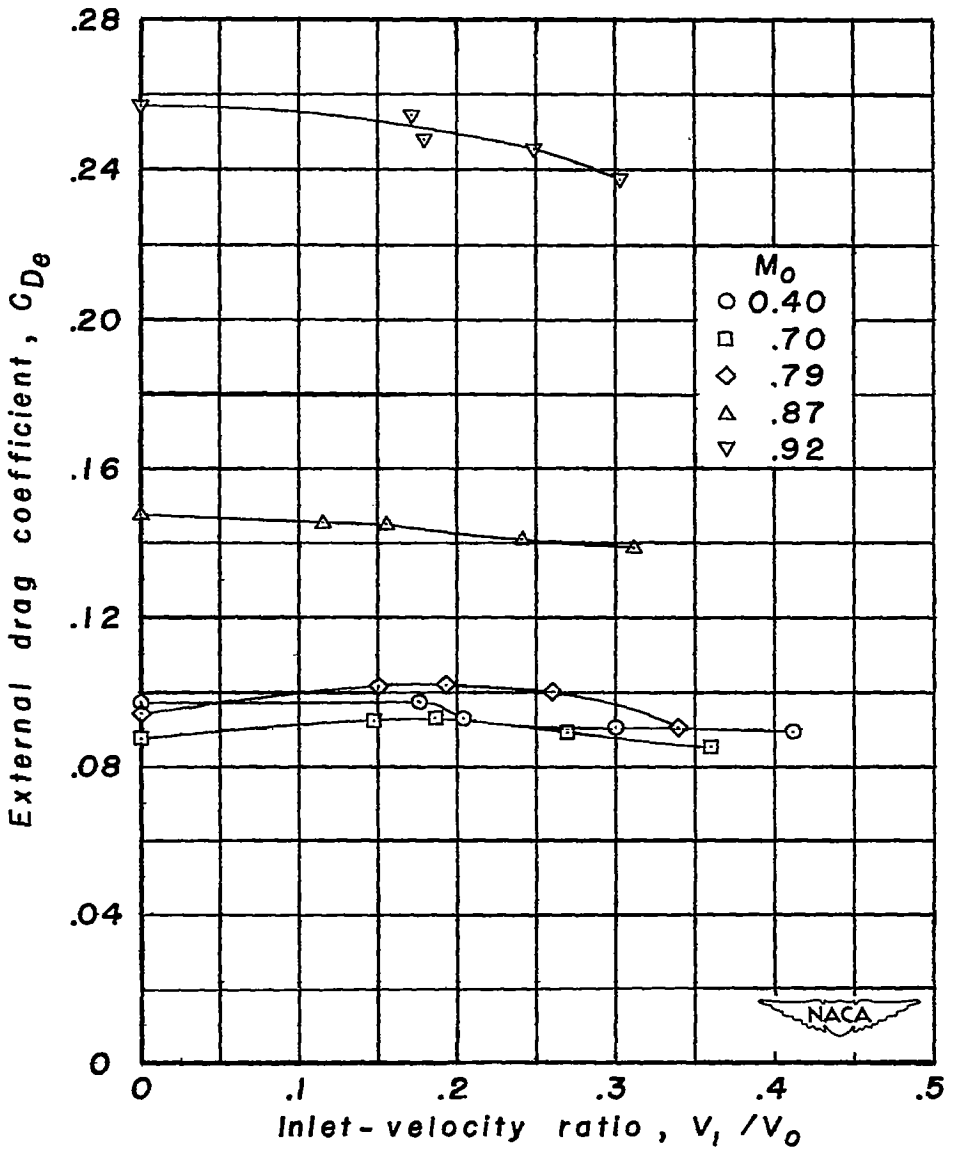

(c) Central body B; $\alpha = 0.1^\circ$.

Figure 12.- Continued.

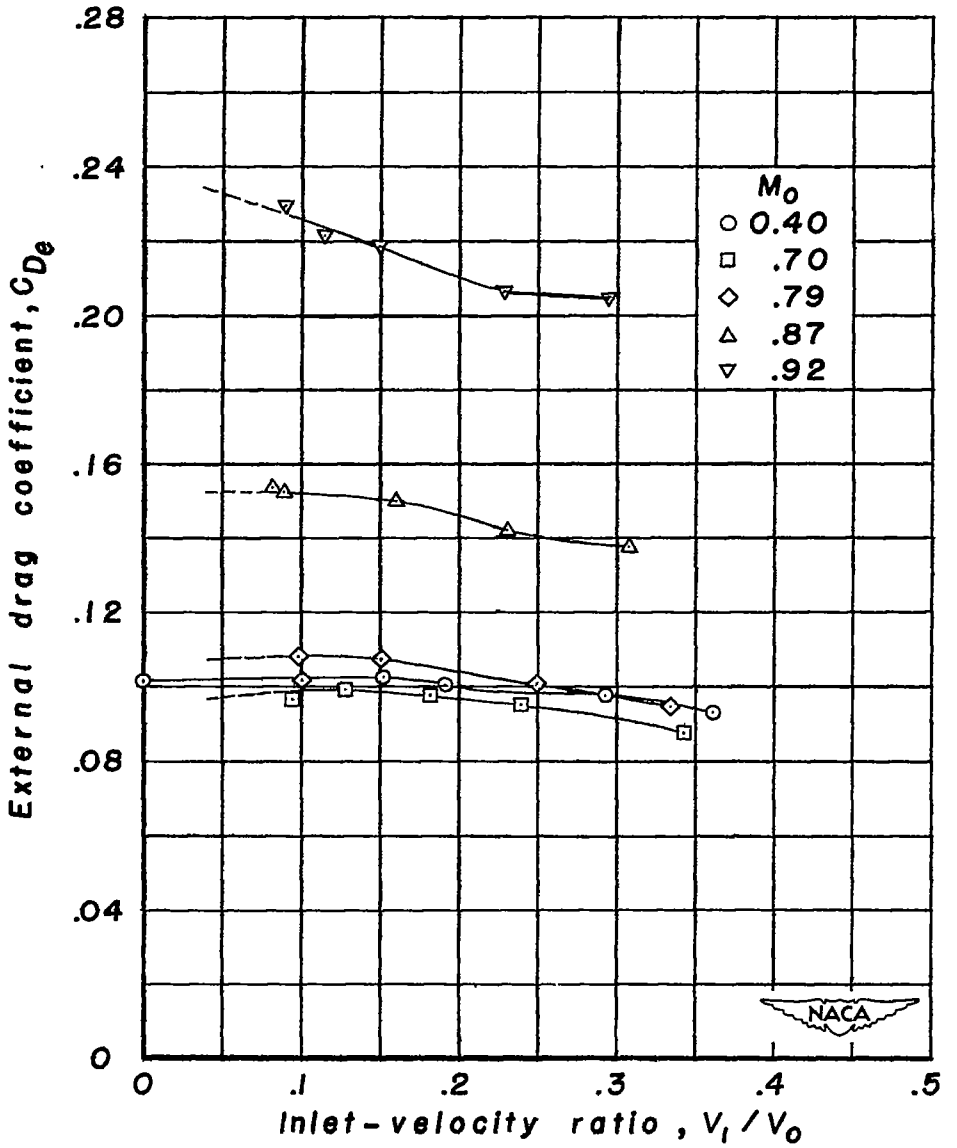

(d) Central body C; $\alpha = 0.1^\circ$.

Figure 12.- Concluded.

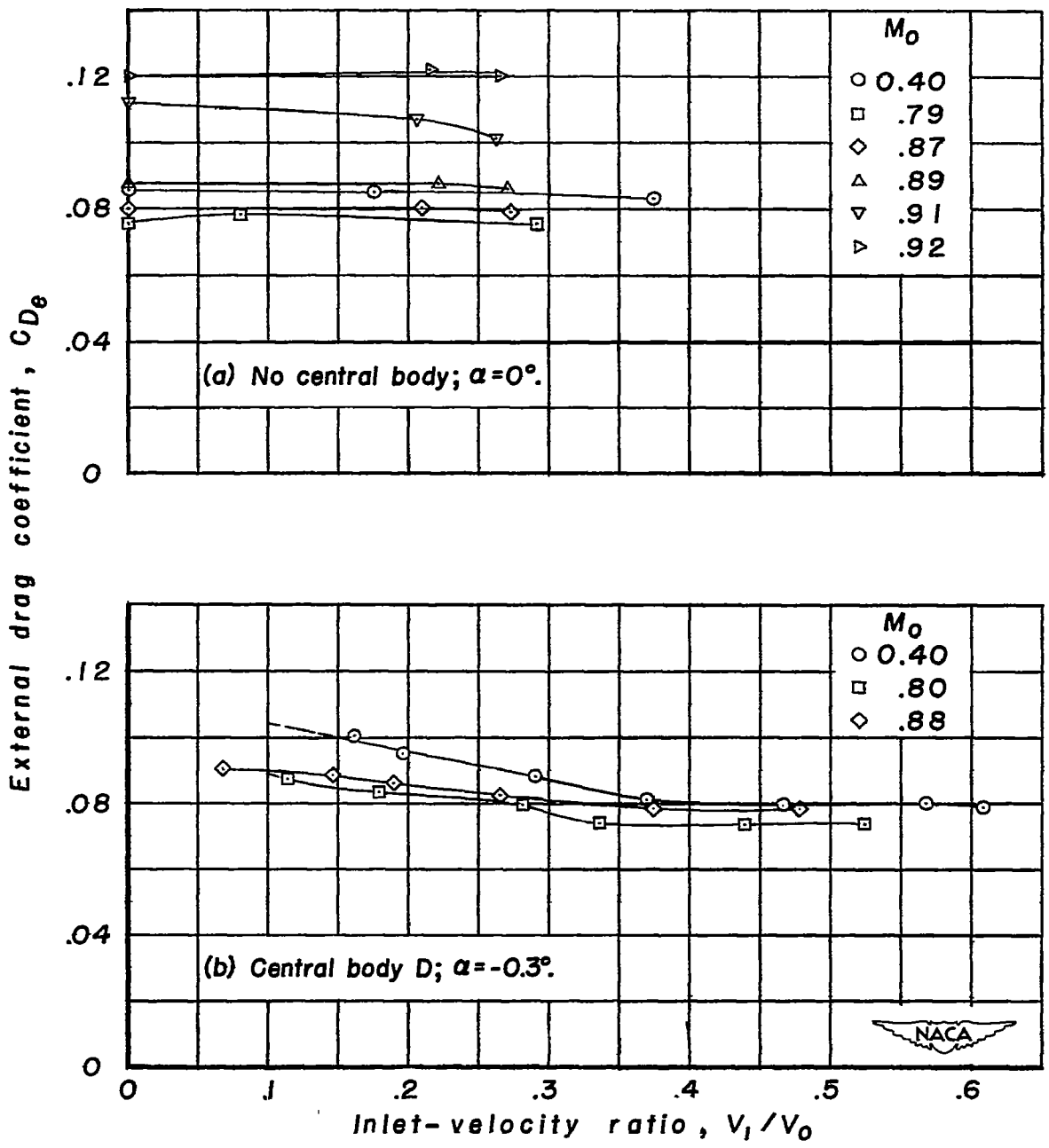

Figure 13.- Variation of external drag coefficient with inlet-velocity ratio. NACA 1-50-100 nose inlet with and without central body.

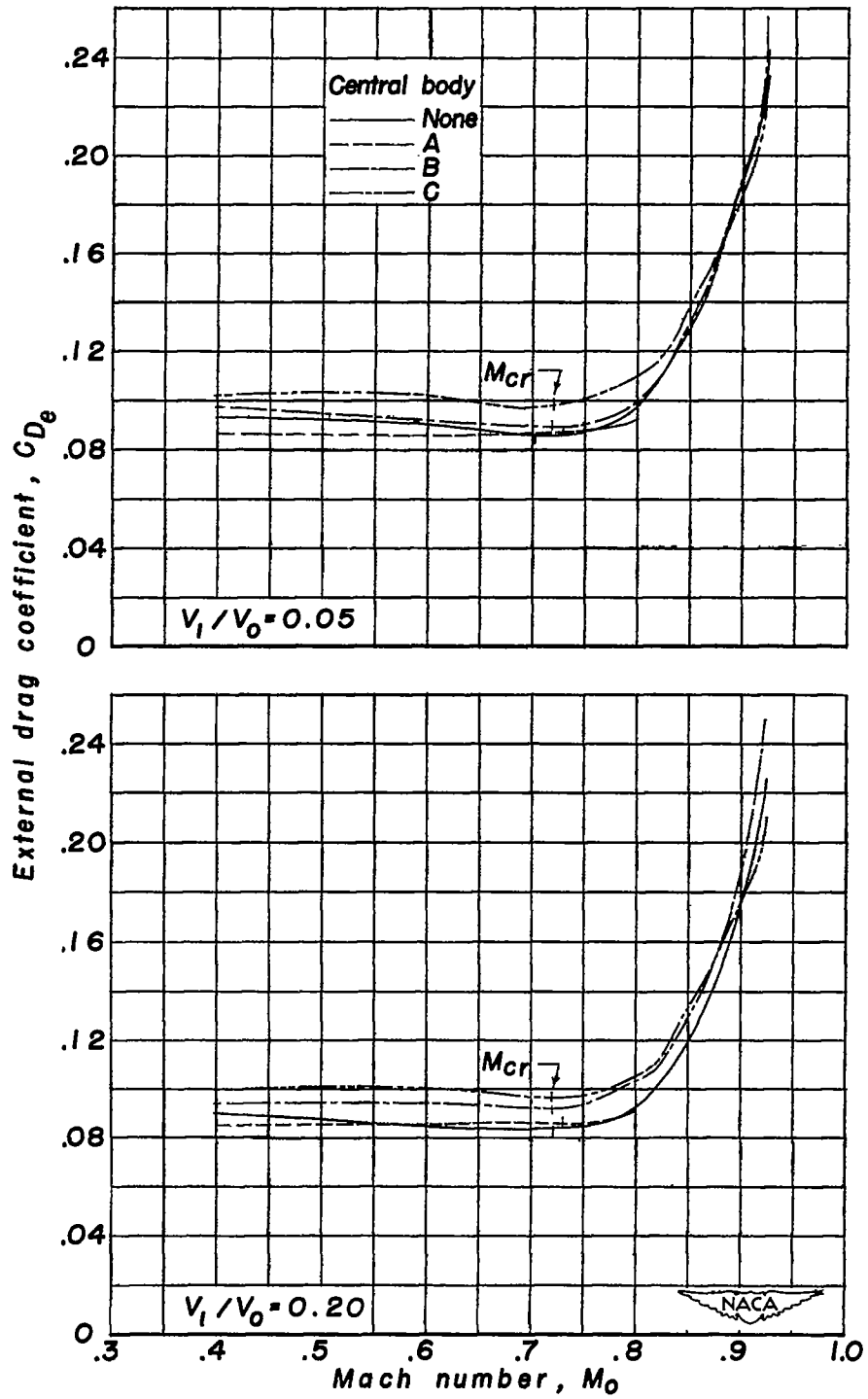

Figure 14.- Effect of central bodies on external drag coefficient. NACA 1-65-050 nose inlet. $\alpha \approx 0^\circ$.

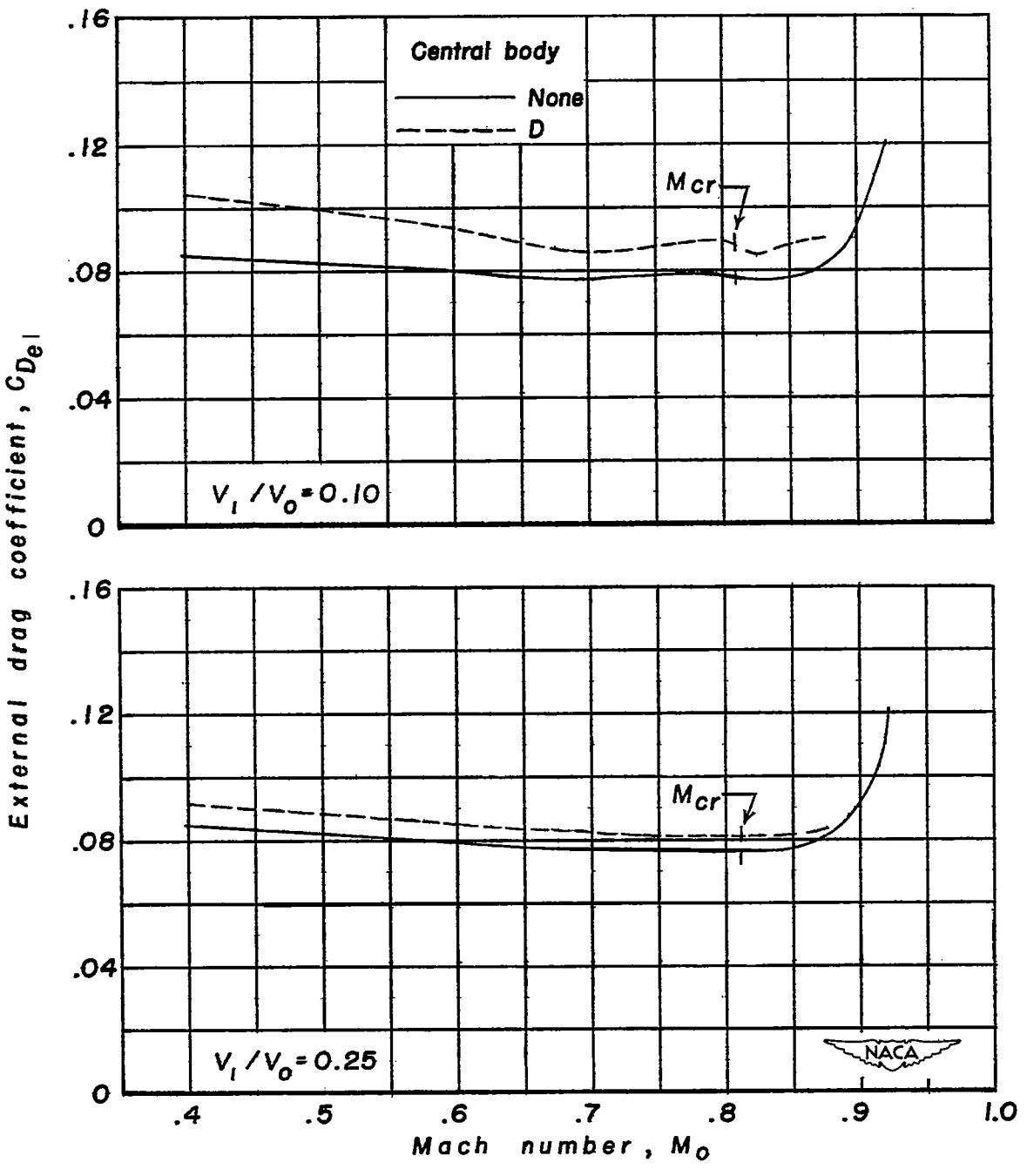

Figure 15.- Effect of central body on external drag coefficient. NACA 1-50-100 nose inlet. $\alpha \approx 0^\circ$.

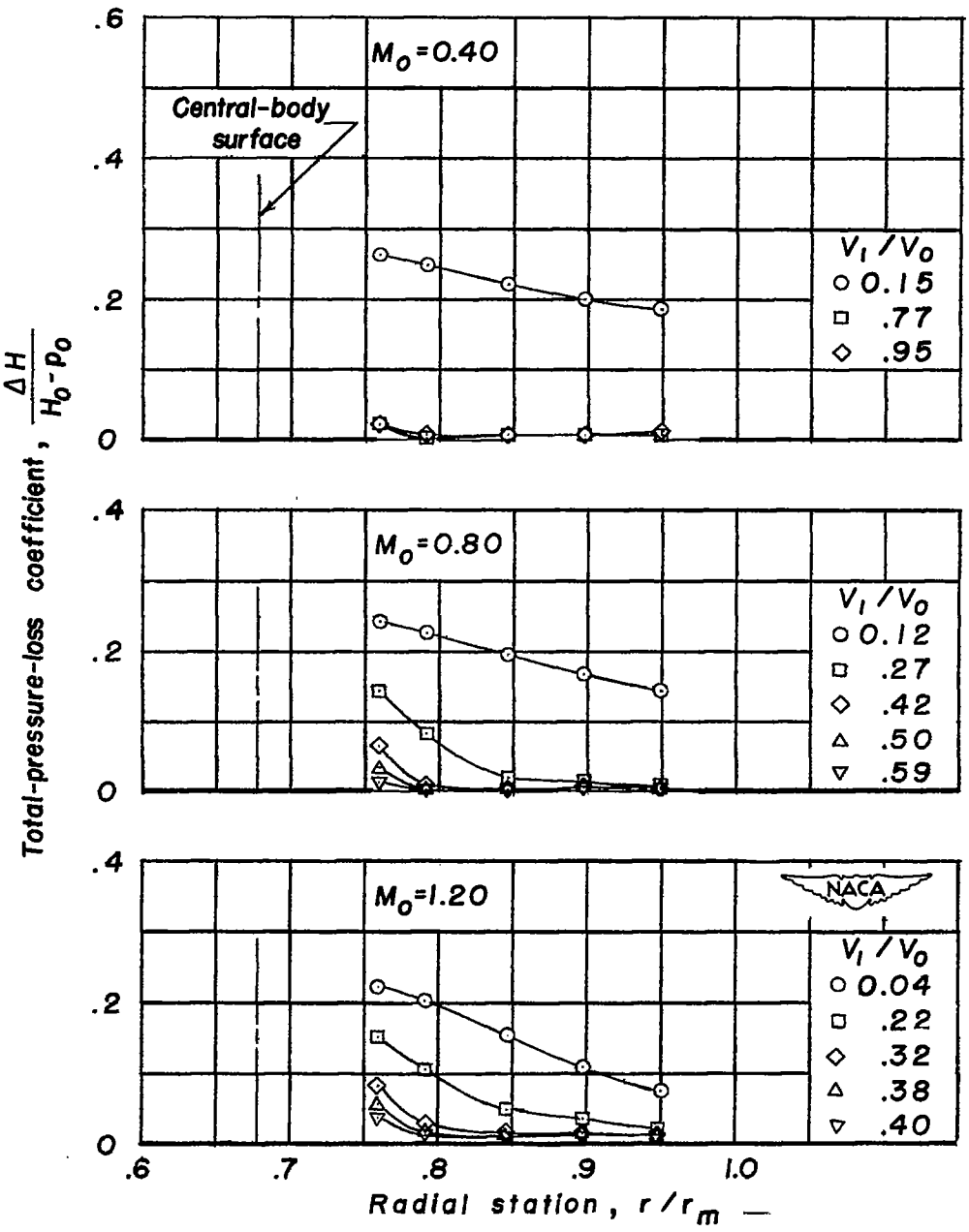

(a) Central body A.

Figure 16.- Distribution of total-pressure-loss coefficient of internal flow near inlet. NACA 1-65-050 nose-inlet - central-body combinations. $\alpha = 0^\circ$.

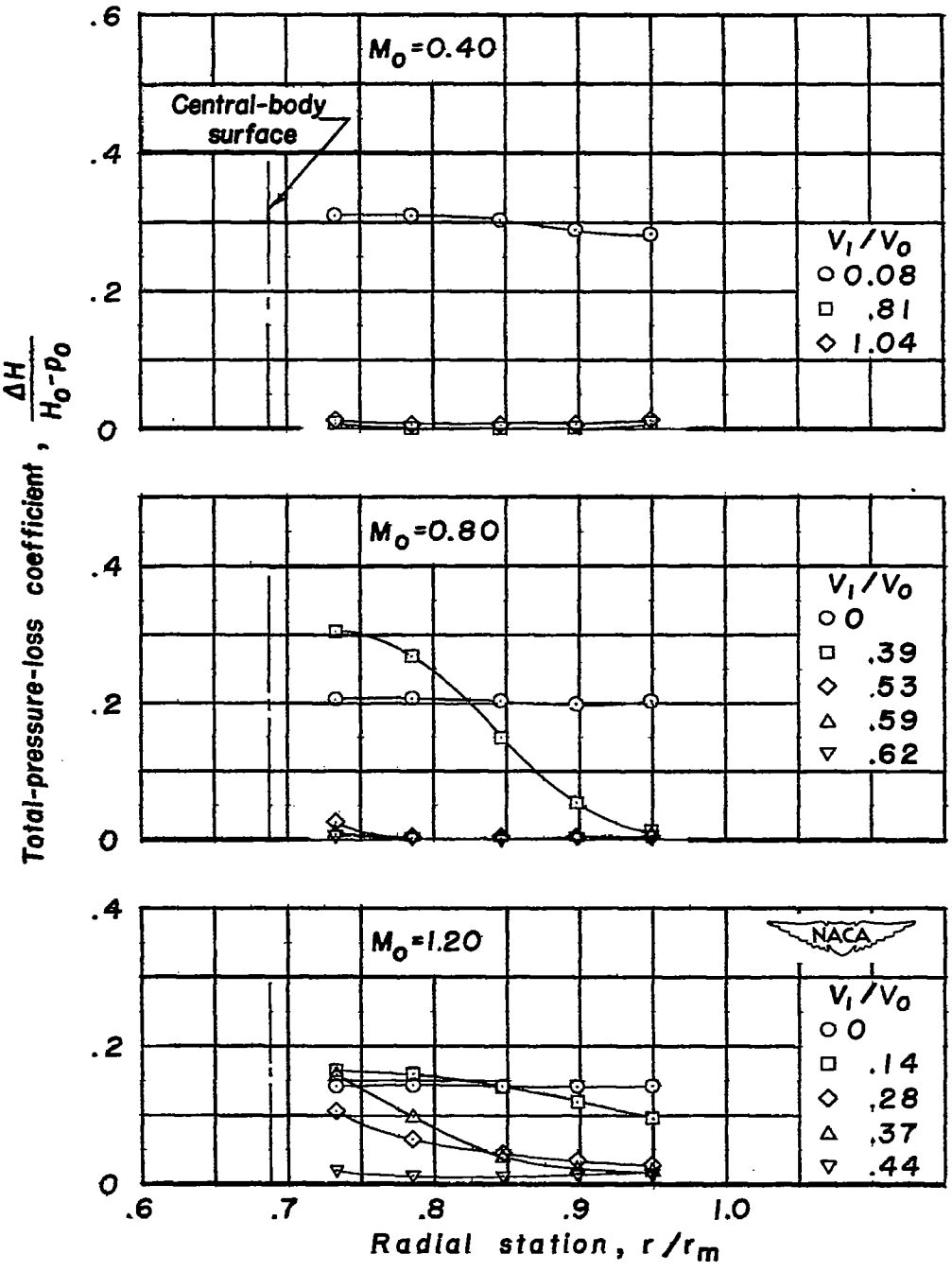

(b) Central body B.

Figure 16.- Continued.

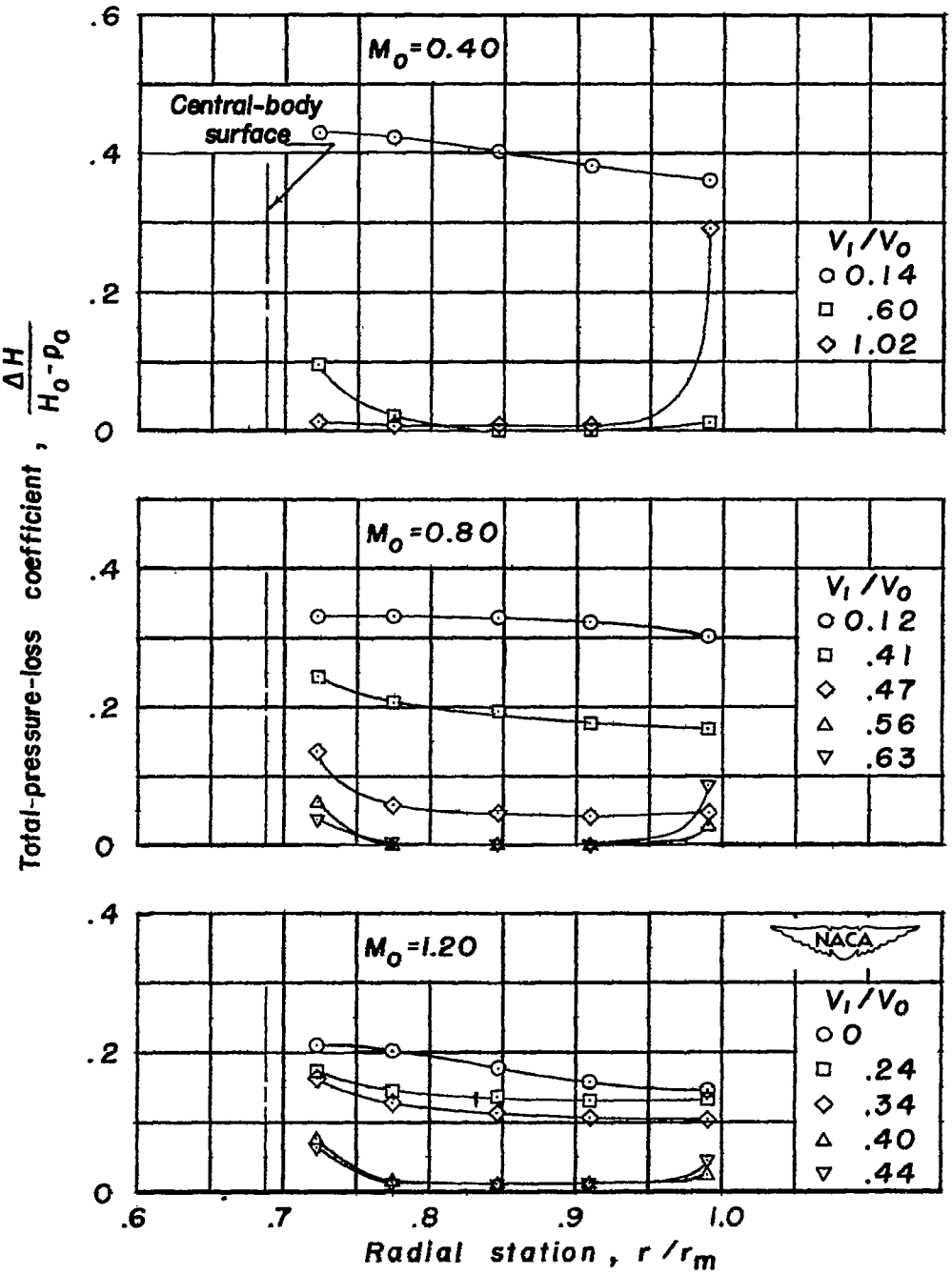

(c) Central body C.

Figure 16.- Concluded.

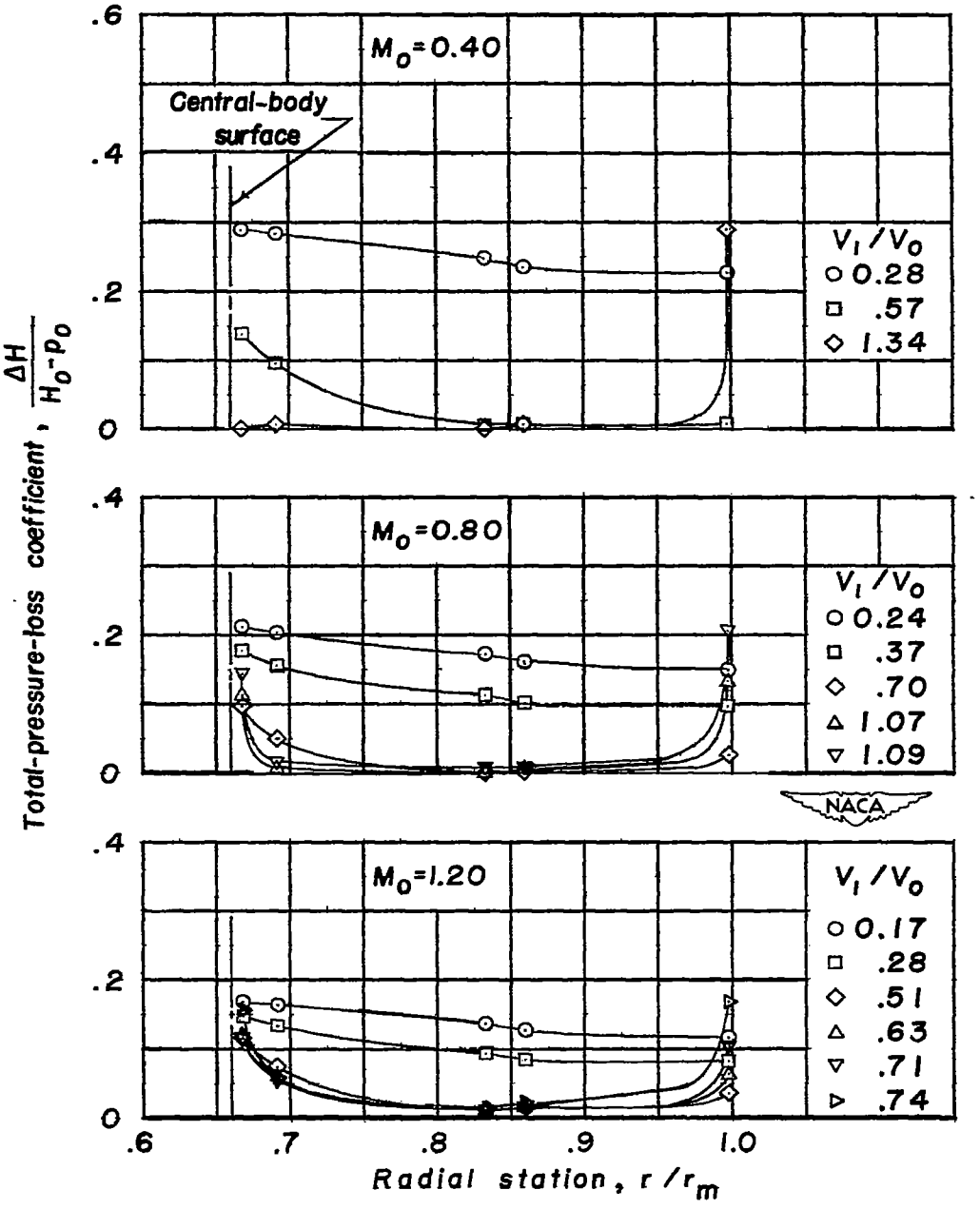

Figure 17.- Distribution of total-pressure-loss coefficient of internal flow near inlet. NACA 1-50-100 nose inlet with central body D. $\alpha = 0^\circ$.

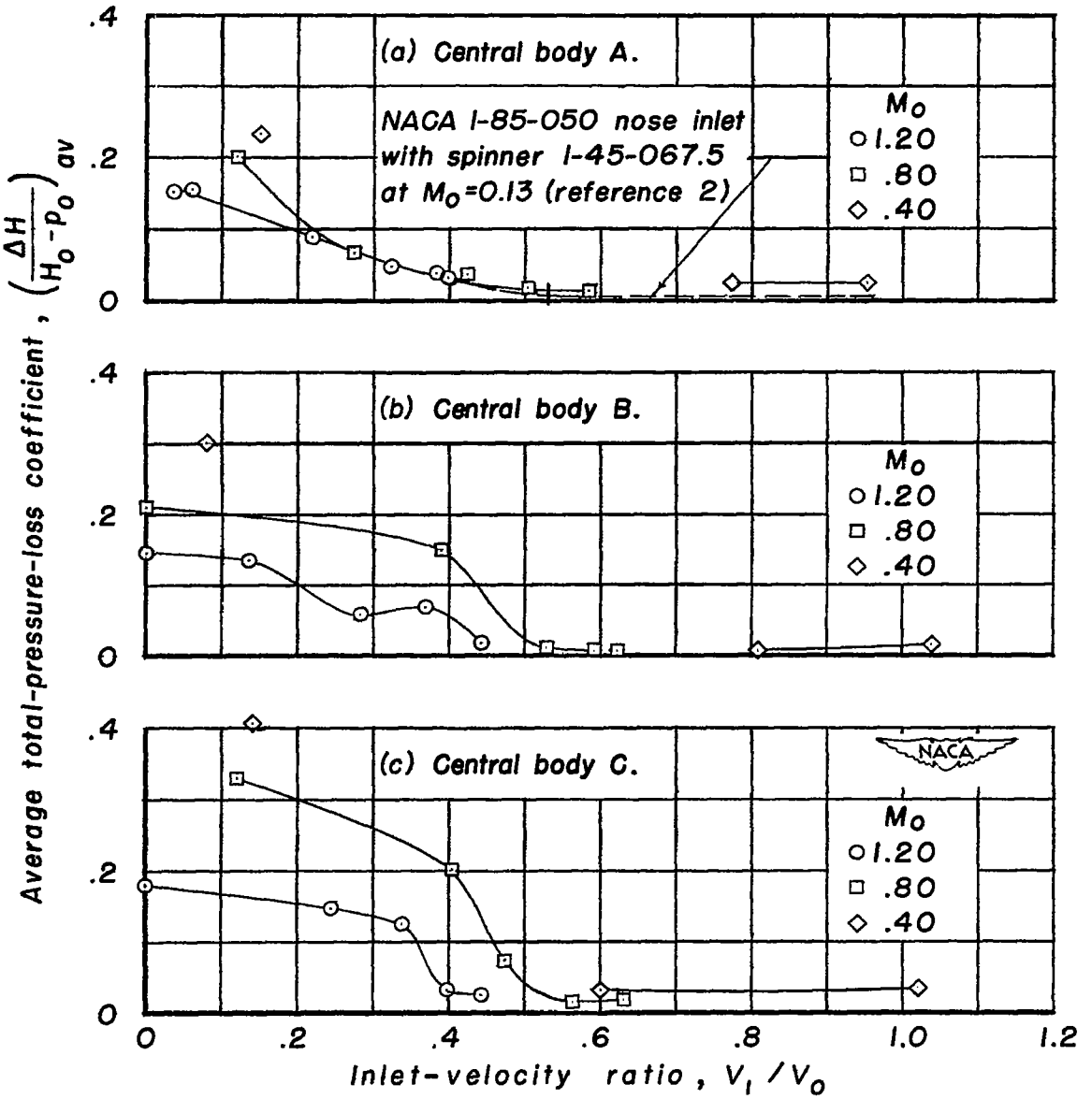

Figure 18.- Variation with inlet-velocity ratio of average total-pressure-loss coefficient of internal flow near inlet. NACA 1-65-050 nose-inlet - central-body combinations. $\alpha = 0^\circ$.

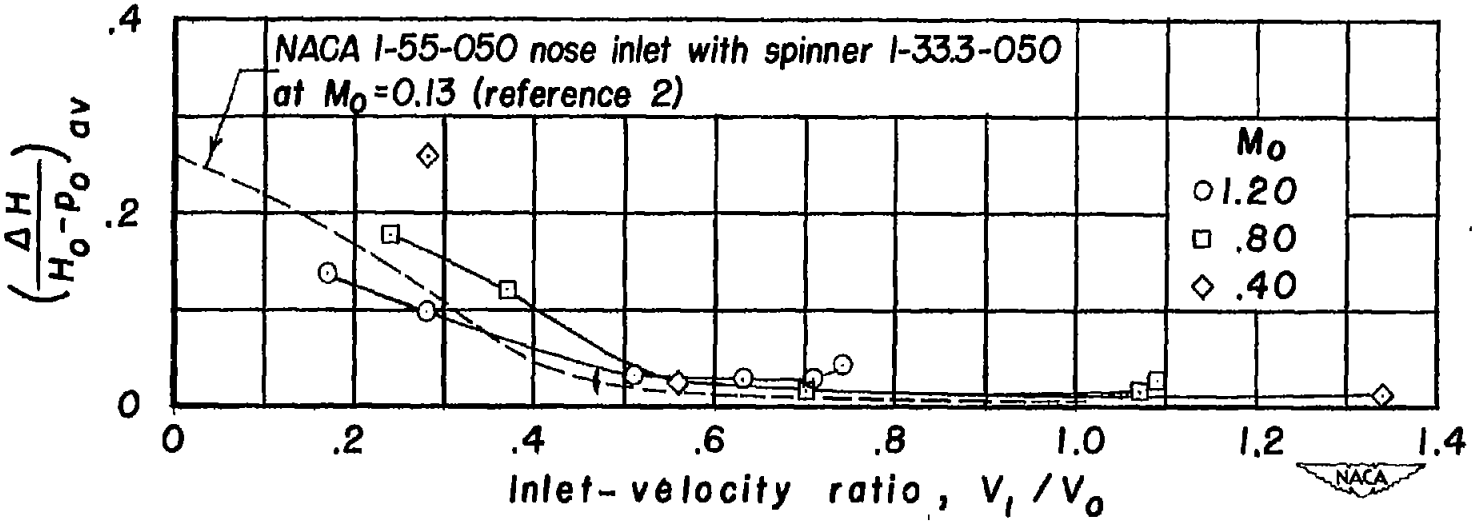

Figure 19.- Variation with inlet-velocity ratio of average total-pressure-loss coefficient of internal flow near inlet. NACA 1-50-100 nose inlet with central body D. $\alpha = 0^\circ$.